Raman study of Cd1–xZnxTe phonons and phonon–polaritons-Experiment and ab initio calculations

T. Alhaddad, M B Shoker, Olivier Pagès, A V Postnikov, V J B Torres, Alain Polian, Y. Le Godec, Jean Paul Itié, Laurent Broch, M.-B. Bouzourâa, et al.

Journal of Applied Physics

AIP Publishing

Raman study of $Cd_{1-x}Zn_xTe$ phonons and phonon-polaritons – Experiment and *ab initio* calculations

T. Alhaddad,[1] M. B. Shoker,[1] O. Pagès,[1,*] A.V. Postnikov,[1] V. J. B. Torres,[2] A. Polian,[3] Y. Le Godec,[4] J.-P. Itié,[4] L. Broch,[1] M. B. Bouzourâa,[1] A. En Naciri,[1] S. Diliberto,[5] S. Michel,[5] P. Franchetti,[1] A. Marasek[6] and K. Strzałkowski[6]

[1] Université de Lorraine, LCP-A2MC, ER 4632, F-57000 Metz, France
[2] Departamento de Fisica and I3N, Universidade de Aveiro, 3810 – 193 Aveiro, Portugal
[3] Institut de Minéralogie, de Physique des Matériaux et de Cosmochimie, Sorbonne Université — UMR CNRS 7590, F-75005 Paris, France
[4] Synchrotron SOLEIL, L'Orme des Merisiers Saint-Aubin, BP 48 F-91192 Gif-sur-Yvette Cedex, France
[5] Institut Jean Lamour, UMR CNRS 7198, Campus Artem, Université de Lorraine, 57078 Metz, France
[6] Institute of Physics, N. Copernicus University, 87-100 Toruń, Poland

[*] Correspondence and requests for materials should be addressed to O.P.
(email: olivier.pages@univ-lorraine.fr)

ABSTRACT

Backward/near-forward Raman scattering and *ab initio* Raman/phonon calculations are combined, together with X-ray diffraction and ellipsometry measurements to further inform the debate on the compact phonon behavior of the II-VI $Cd_{1-x}Zn_xTe$ alloy. The compacity favors the coupling of polar optic modes in both the transverse and longitudinal symmetries via the related ($E_{L,T}$) long-wave electric fields. The E_L-coupling achieves maximum in the Zn-dilute limit which enhances the (upper) ZnTe-like (impurity) mode at the expense of the (lower) CdTe-like (matrix-like) one, leaving the impression of a unique {Cd-Te,Zn-Te}-mixed longitudinal optic (LO) phonon across most of the composition domain. However, the purely-mechanical (non-polar) transverse optic (PM-TO) phonons, that hardly couple, reveal an underlying 3-mode {1×(Cd-Te),2×(Zn-Te)} fine structure that distinguishes between Zn-Te vibrations in Zn- and Cd-like environments up to second neighbors. Further refinement arises by exploring the phonon-polariton (*i.e.*, polar-TO) regime at large Zn content. On reducing the scattering angle, the E_T-coupling develops into a sequential softening of phonon-polaritons from ZnTe- down to CdTe-like ones, which transiently unveils a bimodal pattern behind the Cd-Te signal. Altogether, this results in a (rare) canonical 4-mode {2×(Cd-Te),2×(Zn-Te)} percolation pattern for $Cd_{1-x}Zn_xTe$, *i.e.*, a close II-VI replica of the twin III-V $In_{1-x}Ga_xAs$ one – yet differing by two apparent LO modes and a sensitivity of bond vibrations limited to first-neighbors. Retrospectively, the difference in sensitivity of bond vibrations to the local environment between $In_{1-x}Ga_xAs$ (limited to first neighbors) and $Cd_{1-x}Zn_xTe$ (extending up to second neighbors) emerges as a rule throughout common (covalent) III-V and (ionic) II-VI semiconductor alloys.

I. INTRODUCTION

Basic motivation for a Raman study of $Cd_{1-x}Zn_xTe$. Besides materials' design (down to the nanoscale, through changes in shape and geometry), alloying is a vital track to finely adjust the physical properties of "conventional" semiconductors in view of their targeted applications. Alloying is facilitated by the contrast in structural and mechanical bond properties being low, whereby we refer specifically to bond length (d) and bond covalency (α_c=1$-f_i$, where f_i is the bond ionicity). In particular, α_c is crucial since it governs the ability of a bond to distort under shear stress – measured at the macroscopic scale via the reduced shear modulus (C_s^*) – which directly impacts the stability of the lattice. Interestingly, Vérié[1] has revealed a linear correspondence nicely organized by semiconductor classes (I-VII, II-VI, III-V, IV) between the bond covalency cubed and the structural and mechanical bond properties, captured within the synthetic $C_s^* \times d$ parameter. The ZnTe II-VI compound is special in this classification in that it falls in between the II-VI's and the III-V's. Hence, ZnTe-alloying generates kind of (II-VI,III-V)–hybrid mixed crystals with respect to the structural and mechanical properties, presumably exacerbating also the vibrational properties. In this respect, $Cd_{1-x}Zn_xTe$ is an appealing benchmark for the fundamental study of phonons in mixed crystals in general, as conveniently addressed in laboratory conditions by using optical techniques such as infrared absorption (IR) and Raman scattering.

Among the ZnTe-based mixed crystals, $Cd_{1-x}Zn_xTe$, studied in this work, is further promising for optoelectronic applications – a central issue when dealing with semiconductors – due to its tunable direct optical band gap in the visible (1.45 – 2.26 eV). As electron-phonon scattering adversely affects the optoelectronic properties,[2] it is important before any practical use to characterize the phonons near the center (Γ, q=0) of the Brillouin zone, where photocarriers are generated. IR absorption and Raman scattering are well suited for doing so because they naturally operate near Γ (due to the quasi vertical dispersion of the light probe). This provides a further practical motivation – besides the fundamental one given above – for studying the $Cd_{1-x}Zn_xTe$ phonons via optical techniques.

$Cd_{1-x}Zn_xTe$ phonon mode behavior – Expectations based on (II-VI, III-V) analogies. Our pioneering Raman analysis of $Be_{1-x}Zn_xTe$[3] – even more special than $Cd_{1-x}Zn_xTe$ in the Vérié's classification (see below) – revealed a distinct 4-mode $\{2\times(Zn-Te), 2\times(Be-Te)\}$ pattern falling out of the scope of the two historical models used for the description of the Raman/IR spectra of ternary zincblende mixed crystals, namely the modified-random-element-isodisplacement[4] (MREI) model and the cluster[5] model. By construction, the MREI model is blind to the local environment in that the like bonds of a given species are assumed to vibrate at the same frequency at a given $A_{1-x}B_xC$ composition (1-bond→1-mode, 2-mode in total), irrespectively of inherent fluctuations at the local scale. In contrast, the cluster model actually distinguishes between the vibrations of like bonds depending on their first-neighbor environment, out of four possible ones in a real three-dimension (3D) zincblende crystal (1-bond→4-mode, 8-mode in total) – corresponding to five possible environments for the invariant atom (C), in reference to the number of C-centered tetrahedral clusters (with up to four either A or B atoms at the vertices) involving a given bond . Now, the 2-mode MREI model falls short of explaining the 4-mode behavior of $Be_{1-x}Zn_xTe$, whereas the 8-mode cluster model is clearly oversized.

The disconcerting phonon mode behavior of $Zn_{1-x}Be_xTe$ was explained by introducing our percolation model (Ref. 6 and references therein) that distinguishes between the Zn- and the Be-like environments of a bond (1-bond→2-mode, 4-mode in total), so establishing an analogy with a one dimension (1D) linear chain approximation. In all systems so far examined, phonons are best explained by considering that bond vibrations "feel" their local environment up to first-, or, at most, second-neighbors. This recollects a basic feature of the bond charge model used to describe the phonon dispersions of IV,[7] III-V[8] and II-VI[9] semiconductor compounds in which phonons are essentially a matter of short-range

interactions. In principle, the bimodal pattern per bond (1-bond→2-mode) symmetrically develops throughout the composition domain for both bond species (A-C, B-C) of a $A_{1-x}B_xC$-zincblende mixed crystal. However, in fact, it is well resolved only for the short/stiff/light bond that vibrates at high frequency. This is because the latter bond usually involves the substituent with a small covalent radius, an atom which has much room to displace within its C-cage in order to accommodate the local strain due to the contrast in (A-C, B-C) bond physical properties (length, stiffness), with concomitant impact on the Raman frequencies which get much diversified. The long bond species remains generally blind to the local environment and does not exhibit but a mere MREI-like (1-bond→1-mode) Raman/IR behavior. This results in an apparent 3-mode behavior in total for a disordered zincblende mixed crystal. So far, the percolation model has been applied to all tested II-VI, III-V and IV mixed crystals[10] – explaining all persisting anomalies left unanswered within the MREI/cluster approaches – thereby suggesting its universal character.

The $(\Delta f_i/f_i\,, \Delta d/d)$ mismatches are unusually large (~60%,~9%) for $Be_{1-x}Zn_xTe$ on account that the Be-bonding is highly covalent contrasting with the pronounced ionic character of most II-VI's, to such extent that the Be-based II-VI compounds falls among III-V's in the Vérié's classification.[1] The percolation doublet is well resolved in this case, with a large Be-Te separation of ~35 cm^{-1} apparent in both the Raman[3] and IR[11] data. A Raman doublet shows up also distinctly for the short bond species (Zn-Se) of $Cd_{1-x}Zn_xSe$[10] – with identical substituents as the currently studied $Cd_{1-x}Zn_xTe$ system – even though its f_i–contrast is much lower (~12%) for a similar lattice mismatch (~7%). Conforming to intuition, the doublet is compact in this case, the separation not exceeding ~10 cm^{-1}. As the $(\Delta f_i/f_i\,, \Delta d/d)$ contrasts of $Cd_{1-x}Zn_xTe$ (~24%,~6%) stand in between those of $Be_{1-x}Zn_xTe$ and $Cd_{1-x}Zn_xSe$, we anticipate a distinct percolation Raman/IR doublet for the short (Zn-Te) bond of $Cd_{1-x}Zn_xTe$ as well. In fact, positive signs were lately found by Kozyrev – see below.[12]

Another natural reference for the current discussion of the TO and LO Raman spectra of (II-VI) $Cd_{1-x}Zn_xTe$ is (III-V) $In_{1-x}Ga_xAs$. The substituting and invariant species of both systems are neighbors in the periodic table. The difference (hence contrast) in atomic masses / covalent radii / bond lengths – playing a crucial role in the phonon properties of mixed crystals – is for the both mixed crystals the same (within 1%) and amounts, respectively, to ~40.5% / ~14.5% / ~6.5%.[13] The chemical bonding is (generally) more ionic for II-VI's than for III-V's,[13] resulting in a larger TO-LO splitting. In fact, the splittings for CdTe and ZnTe (~30 cm^{-1}) slightly exceed that for GaAs (~24 cm^{-1}) and InAs (~20 cm^{-1}). Moreover, the contrast in bond ionicity is more pronounced (by roughly a factor of two) for $In_{1-x}Ga_xAs$ (~44%) than for $Cd_{1-x}Zn_xTe$ (~24%),[13] that results in TO-LO bands of the abovementioned III-V parent compounds being well separated (by ~25 cm^{-1}) whereas those in the above II-VI do nearly overlap (the spacing is ~5 cm^{-1}). Nevertheless, alloying enforces the proximity between TO-LO bands in $Cd_{1-x}Zn_xTe$[14] and $In_{1-x}Ga_xAs$.[15] This is due to the local strain (resulting from the contrast in bond length/ionicity) which tilts upward the TO branches on increasing x (along a basic rule that the bond force constant falls down – and hence also the Raman frequency – when a bond is stretched, and vice versa). The difference between the parent and impurity bond lengths in $Cd_{1-x}Zn_xTe$ and $In_{1-x}Ga_xAs$ is revealing in this respect.[13,16,17] Further, in each system the tilts are comparable for both bond species, resulting in quasi parallel TO branches across the composition domain. Though the local strain is similar in both systems, the upward tilt is roughly twice larger for $In_{1-x}Ga_xAs$ (~25 cm^{-1}) than for $Cd_{1-x}Zn_xTe$ (~10 cm^{-1}) – reflecting a larger bond anharmonicity in the III-V than in the II-VI, so that in each system the softening of the upper TO-LO band exactly covers, fortuitously, the frequency gap (large for $In_{1-x}Ga_xAs$ and small for $Cd_{1-x}Zn_xTe$) between the parent TO-LO bands. This ends up with an outstanding feature common for both $In_{1-x}Ga_xAs$ and $Cd_{1-x}Zn_xTe$, that the upper impurity mode (whether GaAs- or ZnTe-like) falls near the lower LO mode of the host lattice (InAs- or CdTe-like, correspondingly). In brief, $In_{1-x}Ga_xAs$ and $Cd_{1-x}Zn_xTe$ are twin systems for what regards their (TO,LO)-Raman behaviors. The point is that the Raman signal of the

stiff/short/light Ga-As bond of $In_{1-x}Ga_xAs$ was recently assigned in terms of a distinct TO percolation doublet, with signs that a similar percolation doublet also exists for the long/heavy In-As species.[3] By analogy, we anticipate a similar percolation fine structure for $Cd_{1-x}Zn_xTe$.

(Non exhaustive) survey on previous $Cd_{1-x}Zn_xTe$ Raman/IR studies. A brief historical survey of the large corpus of experimental $Cd_{1-x}Zn_xTe$ Raman/IR studies – covering a mid-century – is conducted below, separating, for clarity, the Raman and IR insights. We primarily focus on free-standing single crystals grown under equilibrium conditions – using, *e.g.*, the Bridgman method – that are ideal to address intrinsic physical properties owing to these crystals' high quality/purity. Moreover, by applying the magic angle spinning (^{125}Te) solid state nuclear magnetic resonance (NMR) technique, Zamir *et al.*[18] have shown that the Cd↔Zn substitution is ideally random in such crystals (studied at x=0.12, 0.30, 0.50, 0.90), except at small Zn content (x=0.07), in which case a trend towards clustering was evidenced. An overview of existing $Cd_{1-x}Zn_xTe$ (low temperature) Raman and IR frequencies obtained from bulk crystals is given in Fig. 1, as a visual support for the survey. The $Cd_{1-x}Zn_xTe$ epitaxial layers – while conveniently grown on GaAs throughout the composition domain[14] – are not included in Fig. 1 (though not missed in the discussion), due to their comparatively poor crystal quality. Competing nucleation processes during the epitaxy may even lead to phase separation.[19]

It is widely admitted that $Cd_{1-x}Zn_xTe$ exhibits a classical MREI-like 2-mode behavior in its Raman spectra,[12-22] justified by non-overlapping of the CdTe (147 – 169 cm^{-1}) and ZnTe (182 – 210 cm^{-1}) phonon optical bands.[23] However, the available $Cd_{1-x}Zn_xTe$ Raman data in the literature may – to a certain extent – not be fully reliable when it comes to assignment of the nature of phonon modes behavior. This is because such data were acquired in (near) resonant conditions on the E_0 or $E_0 + \Delta_0$ transitions,[24,25] *i.e.*, by driving the study to low temperature (down to liquid nitrogen or liquid helium ones) and by playing with various laser

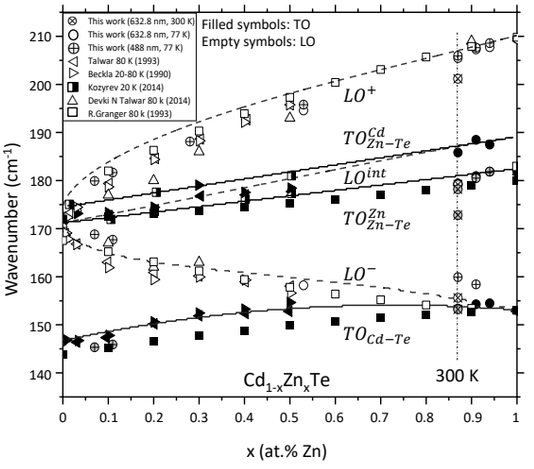

FIG. 1. $Cd_xZn_{1-x}Te$-bulk optical phonon frequencies. Overview of existing IR (squares) and Raman (triangles) TO (filled symbols) and LO (empty symbols) frequencies, in comparison with the current Raman ones (circles). An overall 3-mode description of the underlying $\{TO_{Cd-Te}, TO^{Zn}_{Zn-Te}, TO^{Cd}_{Zn-Te}\}$ pattern is fairly adjusted by considering quadratic (Cd-Te) or linear (Zn-Te) x-dependencies (solid lines). The corresponding (three) LO frequencies obtained via Eq. (1) by assuming a sensitivity of Zn-Te vibrations up to second-neighbors (dashed lines) – in line with Fig. 4 – are added, for comparison with experimental data. The vertical dashed-dotted line refer to room temperature data, as indicated.

lines (LL, spanning the visible) further adjusted depending on composition, along various combinations, *i.e.*, (12K, red laser line, x=0-0.5),[14] (80K, blue-LL, x=0.01-0.3),[26] (80K, blue-LL, x=0.005-0.5, 1),[23] (80K, near-infrared-LL for x=0-0.08, red-LL for x=0.51-0.8, green-LL for x=1),[27] (80K, green-LL, x=0.5, 0.9),[28] (300K, near-infrared-LL for x=0.06, red-LL for x=0.24-0.68)[29] and (80K, blue-LL, x=0.01-0.10 – Ref. 30).

As is well known, resonant Raman scattering selectively enhances the polar longitudinal optic (LO) modes (via the Fröhlich mechanism).[31] The point is that close LO modes – as in the case of $Cd_{1-x}Zn_xTe$[14] – easily couple via their accompanying macroscopic electric field $\vec{E}_L$ (due to the ionicity/polarity of the chemical bonding in a zincblende crystal), which tends to channel the available oscillator strength towards an unique giant feature at high frequency.[32] This results in a levelling-down of Raman signal, suppressing any chance to access the details of the phonon pattern due to a given bond. Seen under this angle, the MREI-like 2-mode behavior proposed for

$Cd_{1-x}Zn_xTe$ on the basis of existing (resonant) Raman studies might be an over-simplification.

For all that, there remain pending issues in the LO symmetry. One refers to the strong emergence of the Zn-Te impurity mode slightly above the Cd-Te matrix one (to be referred to in the following as issue 1). Such abnormal intensity balance between the CdTe- and ZnTe-like LO modes at x~0 subsequently develops into a further disconcerting anomaly that the CdTe-like signal dramatically collapses as soon as departing from the Zn-dilute limit (issue 2). In fact, the CdTe-like LO is hardly visible at ~30 at.% Zn,[29] and quasi undetectable from ~50 at.% Zn onwards (Refs. 23, 27 and 30). Both anomalous features are robust and consistently replicate in all reported Raman data in the literature, being independently detected with epitaxial layers (x~0.1 – Ref. 14, x=0.08 – Ref. 27, x=0.06 – Ref. 29) and single crystals (x=0.01 – 0.03 – Ref. 26; x=0.05, 0.01, 0.03, 0.1 – Ref. 23; x=0.02 – Ref. 30). They are thus presumably intrinsic to $Cd_{1-x}Zn_xTe$ alloying. Yet, they did not attract much attention so far.

To avoid the problem of the LO-coupling, one may shift the focus to the (non-polar) transverse optical (TO) modes. Such purely-mechanical TO modes (PM-TO modes in short) hardly couple and hence preserve the natural diversity of the phonon pattern of a mixed crystal.[10] The PM-TO Raman insight is routinely achieved in the classical backscattering geometry in which the transferred wavevector is at maximum, of the order of 1% of the Brillouin zone size. This falls far away from the (quasi vertical) dispersion of a photon, *i.e.*, the pure transverse electric wave, so that the transverse electric field $\vec{E}_T$ which is likely to accompany the TO mode of a polar crystal (such as a zincblende one) in fact cannot propagate. However, the pure PM-TO Raman insight is currently not available for $Cd_{1-x}Zn_xTe$ – due to the systematic use of near-resonant conditions favoring the LO modes (see above).

Alternatively, an indirect PM-TO insight can be gained by IR absorption, well documented for $Cd_{1-x}Zn_xTe$. The conventional $Cd_{1-x}Zn_xTe$ IR spectra taken at ambient temperature point towards a basic MREI-like 2-mode behavior,[23,33-35] as the LO Raman data. However, a careful examination of the reported IR data reveals a fine structuring behind the Zn-Te signal[12,34,36,37] as well as behind the Cd-Te one.[33,36] The IR fine structure due to a given bond shows up more clearly when the bond is dominant, as emphasized by Granger *et al.*,[38] and can be further clarified by driving the IR analysis down to nitrogen temperature[26] (with no significant difference between 80 – 20 K, as indicated in Ref. 23) – due to sharpening of individual features, or by enhancing spectral resolution when using a synchrotron source.[34,37] Not surprisingly (for reasons given above), in the only reported work combining (resonant) Raman scattering and low-temperature IR reflectivity on the same samples,[26] the fine structuring is visible only in the IR spectra, not in the Raman ones. The IR fine structuring is robust since it consistently reappeared in all subsequent low-temperature $Cd_{1-x}Zn_xTe$ IR studies.[12,36,38,39]

A quantitative insight into the PM-TO modes of free-standing (substrate-free) $Cd_{1-x}Zn_xTe$ single crystals was achieved at moderate Zn content (x=0.28) by Robouch *et al.*[37] using a synchrotron source and by Kozyrev[12] (x=0.01, 0.20, 0.50) at low temperature (20 K). The cited authors extracted the imaginary part of the relative dielectric function reconstructed from a model-free Kramers-Kronig treatment of the raw IR data. This revealed a unique broad Cd-Te mode (~150 cm^{-1}) shifted slightly beneath a pair of close Zn-Te submodes (~175 cm^{-1}) with similar intensities at x~0.25 (Refs. 12, 37), the lower Zn-Te feature becoming dominant (roughly triple) over the upper one at x=0.50 (Ref. 12). Kozyrev stressed that the Zn-Te doublet is so compact (separated by ~4 cm^{-1}) that it could not be resolved in laboratory unless at low temperature.[12]

At the end of this brief overview of the $Cd_{1-x}Zn_xTe$ IR data, we are left with a compact 3-mode $\{1 \times (Cd-Te), 2 \times (Zn-Te)\}$ phonon pattern that may well fall into the scope of the percolation model. Precisely, in his final contribution[12] re-visiting own IR data[36] Kozyrev re-assigned the phonon mode behavior of $Cd_{1-x}Zn_xTe$ in terms of the percolation scenario, the Zn-Te doublet making a distinction between Zn- (lower submode) and Cd-like (upper submode) environments.[12] However, Kozyrev pointed out an apparent

anomaly that the available oscillator strength for the (Zn-Te) doublet does not divide between its two submodes in proportion to $x \cdot (1-x)/x^2$, as observed for the reference (Be-related) doublet of $Zn_{1-x}Be_x$-chalcogenides.[6,10] In fact, the lower/upper Zn-Te submode of $Cd_{1-x}Zn_xTe$ is over/sub-represented (so that, *e.g.*, similar intensities are achieved at x~0.25,[37] and not at x~0.50[10] – as indicated above). Such Zn-Te intensity imbalance cannot be attributed to clustering/anticlustering since the NMR data indicate an ideally random Cd↔Zn substitution in $Cd_{1-x}Zn_xTe$ (at least away from the Zn-dilute limit).[18] It remains an open issue (henceforth issue 3). As for the Cd-Te fine structure observed, *e.g.*, by Granger *et al.*,[38] it is not yet formalized (issue 4).

Last, the phonon-polariton regime remains unexplored in any ZnTe-based mixed crystal so far, constituting an issue *per se* (issue 5).

Objectives of the current study. In this work we perform a Raman study of high quality/purity bulk $Cd_{1-x}Zn_xTe$ single crystals with zincblende structure – ascertained by X-ray diffraction – grown by the Bridgman method at well-spanned x values throughout the composition domain (including the parent systems). Besides the LO modes – already extensively studied in the literature (as detailed above) – the current study further addresses the TO modes, probed both in their non-polar phonon (PM-TO) and polar phonon-polariton (PP) regimes, with *ab initio* (PM-TO) phonon/Raman calculations in support. More generally, our aim is to achieve a consistent understanding of the $Cd_{1-x}Zn_xTe$ Raman/IR spectra covering all (PM-TO, PP, LO) symmetries, and to solve/address all related pending issues (1 to 5).

First, we search for the lacking Raman insight into the reference (non-polar) PM-TO modes of $Cd_{1-x}Zn_xTe$. This is needed to test directly – from the Raman side – the percolation scenario proposed by Kozyrev from his careful IR analysis.[12] The study is placed at large Zn content (x≥0.8) – not yet explored by Raman scattering – corresponding to a high-energy optical band gap (green spectral range), using a low-energy laser excitation (red spectral range, non-resonant). A cooling to liquid nitrogen temperature is further used to improve the resolution of the Raman signal. The discussion of the experimental (non-polar) PM-TO Raman data is supported by *ab initio* calculations of Raman spectra (using the AIMPRO code – Ab Initio Modeling PROgram – Refs. 40 and 41) and/or of the equivalent (in a crude approximation) Γ-projected phonon density of states (Γ-like Ph-DOS, using the SIESTA code – Ref. 42). The SIESTA code is applied to the prototypical percolation-type impurity motif – namely a pair of impurity atoms sitting next to each other – immersed in large (64-atom) parent-like supercells in search for the asymptotic frequencies of the various branches forming the canonical four-mode $\{2\times(Cd-Te), 2\times(Zn-Te)\}$ $Cd_{1-x}Zn_xTe$ PM-TO percolation pattern (in reference to issue 4). A direct insight into the sensitivity of bond vibrations to the local environment – as to whether the sensitivity extends up to first- or second-neighbors, impacting the sharing of oscillator strength between the two submodes forming the Zn-Te doublet, found abnormal by Kozyrev (issue 3)[12] – is tentatively investigated via a subsequent AIMPRO calculation of the PM-TO Raman intensities at intermediate composition (x=0.5) using a large disordered (nominally random) $Cd_{54}Zn_{54}Te_{116}$ supercell.

Next, the attention turns towards the polar modes. The phonon-polariton coupling is explored (issue 5) by near-forward Raman scattering (schematically operating in transmission) at large Zn content where $Cd_{1-x}Zn_xTe$ is transparent to the low-energy (near infra-red, red) laser excitations at hands. Second, the pending LO issues at small-to-moderate Zn content are addressed – referring to the dramatic collapse of the CdTe-like matrix mode on departing from the Zn-dilute limit (issue 2) and to the strong emergence of the ZnTe-like impurity Raman signal at this limit (issue 1). In doing so, we proceed along the linear dielectric approach earlier used by Groenen *et al.* in a similar context with $In_{1-x}Ga_xAs$ – the twin III-V mixed crystal of $Cd_{1-x}Zn_xTe$ – described for the occasion in terms of a crude two-mode $\{1\times(Cd-Te), 1\times(Zn-Te)\}$ MREI-like system.[15] As some percolation-type fine Zn-Te structuring presumably exists for $Cd_{1-x}Zn_xTe$,[12] an intra-bond (Zn-Te) LO-coupling is further considered

besides the inter-bond MREI-like one – for the sake of completeness. In their current versions, the AIMPRO and SIESTA codes cannot handle the macroscopic electric fields carried by the Γ-like LO and PP polar modes. Hence, the LO and PP Raman spectra are modeled analytically within a linear dielectric approach.[43] A crucial ingredient coming into the PP Raman cross section, *i.e.*, the dispersion of the refractive index in the visible (where the Raman scattering operates), is accessed by ellipsometry.

II. SAMPLES, EXPERIMENT, *AB INITIO* CALCULATIONS

A. Mixed crystals

The samples series consists of $Cd_{1-x}Zn_xTe$ single crystals with well spanned x values across the composition domain, including the parent binaries (x=0, 0.07, 0. 11, 0.28, 0.53, 0.89, 0.91, 0.94, 1). The crystals are grown from the melt under equilibrium conditions by using the modified high-temperature and high-pressure vertical Bridgman-Stockbarger method under argon overpressure (about 150 hPa).[44]

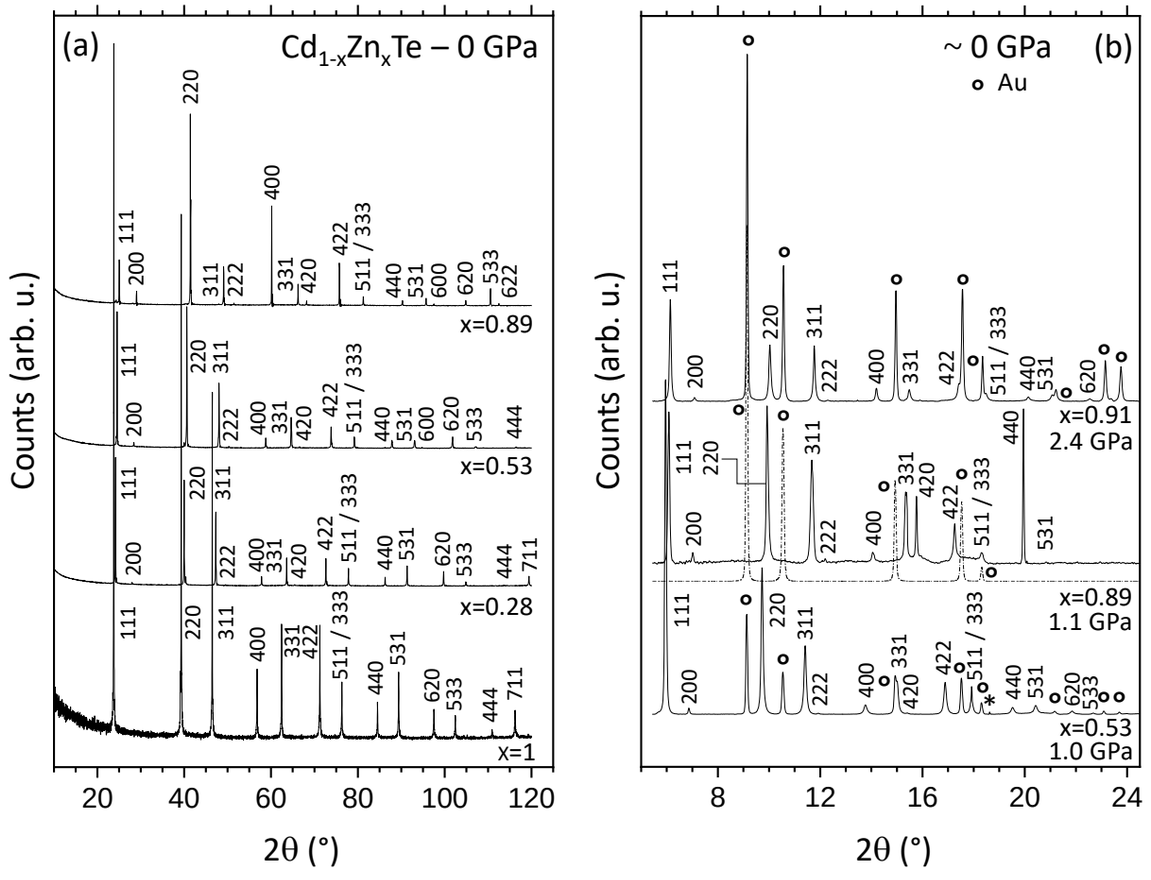

FIG. 2. **$Cd_{1-x}Zn_xTe$ X-ray diffractograms**. Powder X-ray diffractograms obtained at ambient pressure in laboratory with the Cu K-alpha radiation (a) and at nearly ambient pressure (as specified) on the PSICHÉ beamline of synchrotron SOLEIL with the 0.3738 Å radiation (b). Circles mark diffraction lines due to Au used for pressure calibration. In panel (b) the $Cd_{11}Zn_{89}Te$ (solid line) and Au (dashed-dotted line) diffractograms were recorded separately. The star refers to a spurious signal.

The starting materials are mixtures of ZnTe and CdTe powders, each with purity 6N. The studied crystals were cut as cylindrical plates (~1 mm in height, ~3 mm in diameter) from the obtained crystal rods (Ref. 44, see Fig. 2 therein) and polished to optical quality using 1 μm Al_2O_3 powder. The composition x is determined either by energy dispersive X-ray spectroscopy analysis and/or by the induced coupling plasma method, that were checked to be consistent within 1%. The composition gradient along the growth axis of the crystal rods is negligible (less than 0.5 at.% Cd) for the considered height of samples. At any x value the $Cd_{1-x}Zn_xTe$ crystals adopt the same zincblende structure as the binary compounds, as verified by powder X-ray diffraction measurements done either in laboratory conditions at ambient pressure using the Cu Kα line or on the PSICHÉ beamline of synchrotron SOLEIL at (nearly) ambient pressure using the 0.3738 Å radiation – with partial redundancy (x=0.53 0.89) to ensure consistency between the two data sets. The X-ray diffraction peaks exhibit a small linewidth at half height (several arcsec) at any x value, as apparent in Fig. 2, testifying for the high structural quality of all studied crystals.

B. Ellipsometry measurements

A crucial ingredient for the calculation of the phonon-polariton Raman cross section (RCS) in its dependence on the scattering angle is the dispersion $n(\lambda)$ of the refractive index of the studied crystal near the used visible laser excitations. The $n(\lambda)$ dispersion is measured by spectroscopic ellipsometry at large Zn contents where the $Cd_{1-x}Zn_xTe$ mixed crystals exhibit a large optical band gap $E_0(x)$ and hence are transparent to the available laser probes, the *sine qua non* condition to perform near-forward Raman measurements in search for phonon-polaritons. The E_0 values found at room temperature with various samples currently studied by near-forward Raman scattering (including pure ZnTe), identified by first departure from zero of the absorption coefficient – coming off as a by-product of the ellipsometry measurements, are shown in Fig. 3a (symbols). Various laser lines are positioned to appreciate the possible candidates for near-forward Raman measurements. The $E_0 + \Delta_0$ values are added to appreciate by eye the possible resonance conditions, depending on the laser excitation and on composition used.

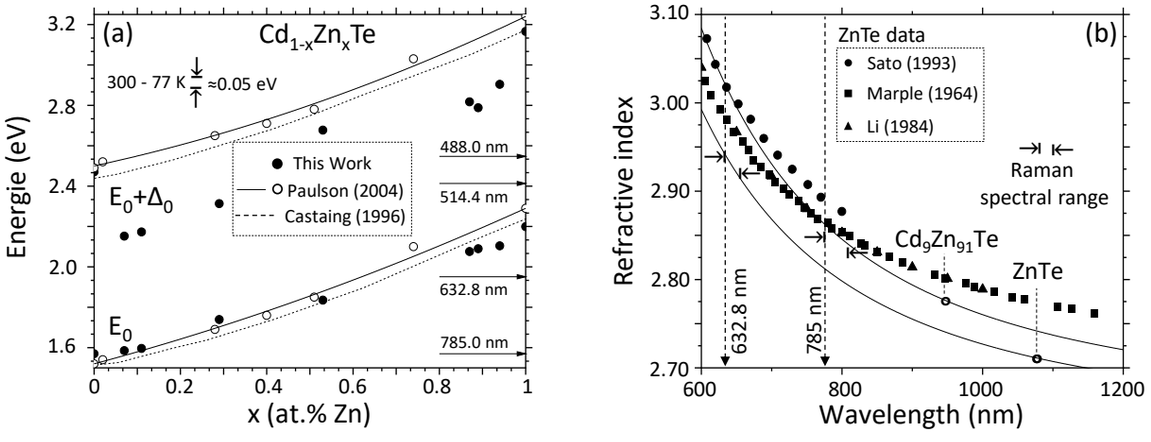

FIG. 3. $Cd_{1-x}Zn_xTe$ main interband transitions and refractive index measured by ellipsometry. (a) E_0 and $E_0 + \Delta_0$ critical transitions. Existing raw data (empty symbols) and/or adjusted trends (dashed and thin lines) are added besides the current data (filled symbols), for comparison. (b) Selected refractive indices below E_0 at large Zn content fitted to the Cauchy formula (lines), used for modeling of near-forward Raman spectra – the addressed spectral range (~200 cm^{-1}) depending on the used laser line (as specified) is emphasized (double arrows). Existing ZnTe data in the literature are added (as specified), for comparison.

The $E_0(x)$ and $(E_0+\Delta_0)(x)$ curves derived from similar ellipsometry measurements throughout the entire $Cd_{1-x}Zn_xTe$ composition domain by Paulson *et al*.[25] (plain lines and squared symbols) and by Castaing *et al*.[24] (dashed lines) are added, for reference.

The raw $n(\lambda)$ curves (symbols) measured from direct (model-free) wavelength-per-wavelength numerical inversion of the spectrometric ellipsometry data (the *sine* and *cosine* of the depolarization angles) below the optical band gap of the two studied crystals (0.91, 1) by near-forward Raman scattering are displayed in Fig. 3b. Analytical forms used in the $Cd_{0.09}Zn_{0.91}Te$ and ZnTe phonon-polariton Raman cross sections are fitted to the Cauchy formula $n^2(\lambda) = A + B \times 10^4 \times \lambda^{-2} + C \times 10^9 \times \lambda^{-4}$ with A, B and C values of (2.655, 10.521 nm^2, 24.313 nm^4) and (2.629, 7.933 nm^2, 18.554 nm^4), respectively, to an accuracy of 5×10^{-4}.

As is well-known, ellipsometry is a very surface[45] and impurity-sensitive[46] technique. In fact, AFM measurements on our samples revealed a significant roughness extending over ~13.6 nm at the sample surface. This roughness, modeled as a mixture of 50% crystal and 50% air using the Bruggeman effective theory,[47] was taken into account in the treatment of our ellipsometry data. This might explain why our $n(\lambda)$ values for ZnTe – used for reference purpose – slightly differ from the reported ZnTe data in the literature[45,46,48] – in which no such surface roughness was considered. The presence of impurities in our crystals as a possible cause for the discrepancy around the $n(\lambda)$ values of ZnTe is ruled out since no absorption is observed in the studied spectral range 600 – 1200 nm. In this range the extinction index values are less than 0.002 by wavelength-by-wavelength numerical inversion and equal to zero by using the absorbing Cauchy dispersion formulas.[49]

C. Backward/forward Raman scattering

The ambition behind the Raman measurements is threefold. First, it is a matter to replicate a pure-LO Raman insight in the Zn-dilute limit (x→0) in view to address quantitatively issues 1 and 2 (see Introduction) with experimental data. Second, we search for the yet missing pure-TO Raman insight in view to tackle the remaining issues 3 and 4 in the non-polar (PM-TO) and polar (phonon-polariton) regimes, studied at small-moderate Cd content where $Cd_{1-x}Zn_xTe$ exhibits a large optical band gap transparent to most visible laser excitations. The advantage is twofold. First, a genuine pure-TO bulk-like Raman signal of such ZnTe-like ($x \to 1$) mixed crystals is achievable without using a (near) resonant laser excitation which would dramatically enhance the spurious LO modes, an unfortunate and unavoidable effect when dealing with CdTe-like mixed crystals ($x \to 0$). Second, transparency is a *sine qua non condition* to address the phonon-polaritons by near-forward (transmission-like) Raman scattering.

In the used backward and forward scattering geometries (see below), a~5mW incident laser beam is focused at the sample surface by using low magnification microscope objective (x4) and lens, respectively, leading to the formation of large laser spots at the sample surface (~100 μm in diameter), which minimizes the power density at the impact spot (~10 mW·m^{-2}). This helps to avoid spurious effects due to sample heating by the laser beam, and notably the formation of Te precipitates with characteristic Raman lines at ~90, ~120 and ~140 cm^{-1} (within 5 cm^{-1}, depending on whether $Cd_{1-x}Zn_xTe$ is mostly CdTe- or ZnTe-like – see Refs. 28 and 27, correspondingly). In fact, no such Te-related peak is observed in the currently reported Raman data, not even under intense Raman cycling while performing the Raman selection rules (Fig. S2, with prefix S standing for Supplemental Material) – see below.

A reference LO Raman overview of our sample series obtained in the backscattering geometry by exciting non-oriented crystals immersed in liquid nitrogen with the 488.0 nm laser line of an Ar^+ laser line near-resonant either with the E_0 transition or with the $E_0 + \Delta_0$ one at large Zn and Cd contents, respectively,[24,25] testified by activation of LO-harmonics up to the third order (at least) is separately provided (Fig. S4). The reported data replicate earlier ones taken by Aydinli *et*

al.[27] (Fig. 2 therein) under similar conditions, and are further consistent with less-resolved ones – especially at moderate-small Zn content – recorded at room temperature by Znamenschykov *et al.*[29] (Fig. 4 therein).

Novel TO-like Raman spectra probing the PP's and/or their native PM-TO's are recorded at room and/or nitrogen temperatures in the near-forward and backward scattering geometries by directing the non-resonant 632.8 nm and/or 785.0 nm radiation(s) through/onto high-quality (110)-oriented crystal faces obtained by cleavage. In the former (near-forward) scattering geometry, the scattering angle between the wavevectors of the incident laser beam and of the scattered light inside the crystal, *i.e.*, $\theta = (\widehat{\vec{k}_i, \vec{k}_s})$, is varied by slightly departing the laser beam from normal incidence ($\theta = 0°$) at the rear crystal face, while maintaining the detection of the scattered light along the $\vec{Z}$-$[110]$ direction perpendicular to the top crystal face.

The vibrational quality of our crystals is tested by studying the PM-TO Raman selection rules – using the same setup as detailed in Ref. 50. The polarized Raman spectra are labeled by using the PorTO modes notation $\vec{k}_i(\vec{e}_i, \vec{e}_s)\vec{k}_s$,[51] in which the wavevectors (outside the brackets) and polarizations of the incident and scattered light, specified via explicit subscripts, are expressed in the laboratory coordinate system coinciding with the $\vec{X} = [\bar{1}10]$, $\vec{Y} = [001]$ and $\vec{Z} = [110]$ crystal axis. The experimental dependencies of the crossed- and parallel-polarized Raman intensities on the azimuth angle $\alpha = (\widehat{\vec{e}_i, \vec{X}})$ at the sample surface are discussed in reference to the theoretical $(\vec{X}, \vec{Y})$-centered Greek cross-like and butterfly-like patterns, respectively.[50]

The contour modeling of the $PM-TO$, PP and LO $Cd_{1-x}Zn_xTe$ Raman lineshapes is achieved by using the following updated version of our generic Raman cross section (RCS) derived in Ref. 52 in which the x-variations of all alloy-related $PM-TO$ frequencies (used as input parameters) are explicitly taken into account, *i.e.*,

$$RCS \sim Im\left\{\left(-\frac{1}{\Delta(\omega,q,x)}\right)\times\left[1+\sum_p C_{p(x)}\times L_p(\omega,x)\right]^2 + \sum_p C_p^2(x)\times S_p^{-1}(x)\times L_p(\omega,x)\right\}, \quad (1)$$

derived by adapting to a discrete assembly of polar phonons the linear dielectric approach originally used by Hon and Faust to formalize the phonon-plasmon polar coupling (in GaP).[43] The polar phonons can be either decoupled (PM-TO modes, $\varepsilon_r \to \infty$), coupled via a longitudinal electric field (LO modes, $\varepsilon_r = 0$), or coupled via a transverse electric field (PP's, $\varepsilon_r = q^2c^2\omega^{-2}$), impacting the resonance term ($\Delta(\omega, q, x) = \varepsilon_r(\omega, x) - q^2c^2\omega^{-2}$). In either case, the relative dielectric function $\varepsilon_r(\omega, x)$ of $Cd_{1-x}Zn_xTe$ plays a central role (as specified within brackets). We adopt a classical form including an electronic background, *i.e.*, $\varepsilon_\infty(x)$, besides Lorentzian-like $L_p(\omega, x)$ contributions from the various phonon modes, *i.e.*, p in total, depending on the used MREI- (p=2) or percolation-type (p=3-4) description of phonon mode behavior. Each Lorentzian is characterized by its resonance at the p-related $PM-TO$ frequency, noted $\omega_{T,p}(x)$, by its (sample-dependent) damping $\gamma_p(x)$ governing the full width at half maximum, and by its oscillator strength $S_p(x)$ that controls both the magnitude of the p-related $TO-LO$ splitting and the Raman intensities of all p-type ($PM-TO$) modes. The p-related Faust-Henry coefficient, noted $C_p(x)$, that measures the relative Raman scattering efficiencies of the non-polar (PM-TO) and polar (LO, PP) p-type modes, is involved in the RCS as a weighting factor of the main $\varepsilon_r(\omega, x)$-related term and thus also contributes to the p-related Raman intensities.

Most input parameters refer to the parent CdTe and ZnTe systems. Together with ε_∞ – the high frequency relative dielectric constant – the PM-TO (ω_{TO}) and LO (ω_{LO}) Raman frequencies define the parent oscillator strengths (noted S_{CdTe} and S_{ZnTe}, given by $\varepsilon_\infty \cdot \Omega^2 \cdot \omega_{TO}^{-2}$, with $\Omega^2 = \omega_{LO}^2 - \omega_{TO}^2$).[4] The remaining parent parameters are the Faust-Henry coefficients (noted C_{CdTe} and C_{ZnTe}). The used (ε_∞, ω_{TO}, ω_{LO}, C) values for CdTe and ZnTe at nitrogen temperature are (7.3,[23] 146.4 cm^{-1}, 170.3 cm^{-1}, -0.14[53]) and (7.2,[23] 182.0 cm^{-1}, 211.0 cm^{-1}, -0.11[54]), respectively, assuming invariance of the C values with temperature (in the studied 77 – 300 K range). The non referenced parameters are directly measured in this work.

The only alloy-related input parameters are the frequencies and dampings of the PM-TO modes, *i.e.*, $\omega_{T,p}(x)$ and $\gamma_p(x)$, being directly observable in the backscattering geometry. As for $S_p(x)$ – Ref. 4 and $C_p(x)$ – Ref. 15, they scale linearly with the fraction $f_p(x)$ of oscillator-p in the crystal (given in the course discussion), reflecting the gradual collapses of the TO-LO frequency gap and of the scattering mechanism due to the macroscopic electric field of a LO mode, respectively, when the corresponding mode gets more and more dilute/localized in the crystal, until the LO eventually assimilates with its native PM-TO in the impurity limit.

D. *Ab initio* AIMPRO and SIESTA calculations

An *ab initio* insight into the asymptotic $\omega_{T,p}(x)$ frequencies of the presumed four PM-TO $[2\times(Cd-Te), 2\times(Zn-Te)]$ branches (p=4) in the nominal "ω *vs.* x" percolation plot of $Cd_{1-x}Zn_xTe$ are gained by applying the Siesta code to the minimal percolation-type impurity motif, namely a duo of Zn (x~0) or Cd (x~1) impurities connected via Te, immersed in large 2x2x2-replicated (64-atom) zincblende-type CdTe- and ZnTe-like supercells, respectively.[55] The impurity motifs are well separated under the supercell-imposed periodicity, fairly representing the "isolated defect" situation. The Siesta calculations are concerned with the phonon density of states projected at the centre Γ of the Brillouin zone (Γ-projected Ph-DOS) that assimilates with the PM-TO Raman signal in a crude approximation. The calculations are done within the frozen-phonon technique after full relaxation (lattice constant and atom positions) of the supercell.

The Siesta calculation setup was described earlier, *e.g.*, for the $Cd_{1-x}Zn_xSe$ system.[10] The norm-conserving pseudopotentials has been constructed using the scheme of Troullier and Martins[56] for the following set of nominal charge configurations and the pseudoization radii (the numbers in brackets, in Bohr units, following the corresponding electron shell label): $5s^2(2.47)5p^0(2.60)4d^{10}(2.40)4f^0(2.40)$ for Cd, $4s^2(2.43)4p^0(2.37)3d^{10}(2.10)4f^0(2.82)$ for Zn, $5s^2(2.00)5p^4(2.58)4d^{10}(1.80)4f^0(2.50)$ for Te. The basis functions of the "double-zeta with polarization orbitals" quality were generated using the "energy shift" parameter, which controls in Siesta the confinement of the basis functions, equal to 10 mRy. This resulted in the following values of the maximal extension of strictly confined orbitals (the most protruded ones on each atom): 3.36 Å for Zn, 3.55 Å for Cd, 3.36 Å for Te. The exchange-correlation was treated within the local density approximation (LDA), whereby no special effort was taken to correct for the band gap value. The force constants in phonon calculations are slightly overestimated, resulting in a slight upward drift of the calculated frequencies by ~15 cm^{-1}, as compared to experimental results – see below. The k-sampling was done over 4x4x4 divisions of the (cubic) Brillouin zone of the supercell, that was tested to yield sufficient accuracy in the calculation of forces.

Further *ab initio* insight into the relative Raman intensities of the like PM-TO modes forming the CdTe- and ZnTe-like percolation-type Raman doublets of $Cd_{1-x}Zn_xTe$ is searched for by calculating the genuine PM-TO Raman signal using the AIMPRO code. This is interesting notably in view to shed light upon the sensitivity (whether it ranges to first or second neighbors) of such vibrations to their local Zn- (lower mode) or Cd-like (upper mode) environment. The study is placed at intermediary composition (x=0.5) where both bond species and both local (Cd- and Zn-like) environments are well represented, using the same large 216-atom zincblende supercell optimized to a random substitution by simulated annealing as recently tested with $Cd_{1-x}Zn_xSe$.[57]

The AIMPRO Density Functional Theory calculations were done within the LDA for the exchange-correlation potential by Perdew and Wang,[58] taking the norm-conserving pseudopotentials for Cd, Zn and Te as proposed by Hartwigsen, Goedecker and Hutter.[59] The 3*d* and 4*d* electrons were taken into account explicitly as valence electrons for Zn and Cd, respectively. Kohn-Sham orbitals were expanded in atom-centered *s*, *p* and *d* cartesian-gaussian functions. The Brillouin zone of the 216-atom cubic supercell was sampled by $2\times2\times2$ special k-point mesh as proposed by Monkhorst and Pack.[60] The lattice

parameter (a), the bulk modulus (B_0) and the first pressure derivative of the bulk modulus (B') were obtained for the reference crystals using a third-order Birch-Murnaghan[61] equation of state. This approach gives a = 0.602 (0.644) nm, B_0 = 54.2 (45.7) GPa and B' = 4.7 (4.8) for ZnTe (CdTe), respectively. These theoretical values are in reasonable agreement with the ZnTe (CdTe) experimental data of a = 0.609 (0.648) nm and B_0 ~52.8 (44.5) GPa, as well as with other *ab initio* calculations of B' ~ 4.65 (4.77), respectively.[62-65]

The *ab initio* Raman cross section was calculated following de Gironcoli,[66]

$$\sigma^{xy}(\omega) \propto \sum_{\nu} \frac{\delta(\omega_\nu - \omega)}{\omega_\nu} \left|\sum_i s_i \, u_{iz}^{\nu}\right|^2 \qquad (2)$$

where ν runs through all phonon modes, ω_ν is the frequency of the ν mode, u_{iz}^{ν} the z component of the displacement of the atom at the lattice site i and mode ν, s_i is +1 and -1, depending on whether the site i belongs to the cationic or anionic fcc sublattice, respectively. $\delta(\omega_\nu - \omega)$ was considered to be a 2 cm^{-1} – broad Lorentzian function. The AIMPRO code calculates the second order partial derivatives of the total energy with respect to the atomic coordinates at equilibrium positions. The frequencies and the normal modes were obtained by diagonalization of the dynamical matrix. The equilibrium configurations were determined after an exhaustive full relaxation (atom positions and lattice parameter), until the maximum force was 0.1 meV/Å. The AIMPRO code uses downhill simplex optimization to minimize the total energy with respect to the lattice parameter, and a conjugate gradient method to relax the atomic positions.[67] For the parent crystals ZnTe and CdTe, the calculated $PM-TO$ Raman frequencies of ~191.9 cm^{-1} and ~151.6 cm^{-1}, respectively, are in good agreement with available experimental data for ZnTe (~ 182 cm^{-1} in Ref. 68 and ~182 cm^{-1} in this work) and CdTe (~170.0 cm^{-1} in Ref. 69 and ~145.0 cm^{-1} in this work).

III. PERCOLATION-BASED *AB INITIO* PM-TO INSIGHT INTO THE PHONON MODE BEHAVIOR OF $Cd_{1-x}Zn_xTe$

The canonical $\{2\times(Cd-Te), 2\times(Zn-Te)\}$ PM-TO version of the $Cd_{1-x}Zn_xTe$ percolation scheme is governed by four asymptotic $\omega_{TO,p}(x)$ frequencies at x~0 and 1 determined via a Siesta calculation of the Γ-projected Ph-DOS per atom, related to parent-like supercells containing a duo of neighboring impurities (2-Imp.). The isolated impurity (1-Imp.) is also considered for reference purpose (not shown). The 2-Imp. (duo) Γ-projected Ph-DOS per atom flank the both sides of the main (a) panel in Fig. 4. The actual 3D vibration patterns are sketched out (on the right), for clarity. Their discussion is transposed at 1D hereafter for the sake of consistency with the 1D percolation scheme.

Consider, *e.g.*, the Zn-Te branches at x→0. The 1-Zn motif in CdTe gives rise to a triply degenerate Zn-Te impurity mode, abbreviated CdTe:1Zn, due to Zn-Te vibrations in a Cd-like environment. This assimilates with the asymptotic limit of TO_{Zn-Te}^{Cd} at x→0. The five out-of-chain modes of the Zn-duo vibrating in similar way are in fact, within the 1D paradigm and notation, the Zn-Te vibrations in presence of Cd, and hence, in principle, ought to be degenerated with CdTe:1Zn. The remaining Zn-Te vibration within the 2Zn-duo (in-chain), noted CdTe:2Zn, refers to Zn-Te vibrating "in its like" Zn-environment, hence to be identified with the asymptotic limit of TO_{Zn-Te}^{Zn} at x→0. The 2-Zn and/or 1-Zn motifs are further useful to fix the Cd-Te doublet at x→0. Basically, the Cd-Te vibrations away from and close to 2-Zn/1-Zn, correspondingly abbreviated CdTe and CdTe/Zn, reveal the asymptotic TO_{Cd-Te}^{Cd} and TO_{Cd-Te}^{Zn} limits, respectively.

As the CdTe and ZnTe PM-TO modes are nearly dispersionless,[9] the ranking of the above four asymptotic frequencies at x→0 is solely governed by the local strain.[32] The Zn-Te bond is shorter than the Cd-Te one, so that the Cd-Te bonds close to one Zn suffer a tensile strain. Hence, CdTe/Zn vibrates at a lower frequency than pure CdTe (x=0), and, vice versa, the isolated short Zn-Te bond suffering a tensile strain from the CdTe-like host matrix (x~0) vibrates at a lower frequency than in pure ZnTe

(x=1). The high-symmetry (isotropic) 1-Zn motif is more efficient than the less symmetric 2-Zn (quasi uniaxial) one in accommodating the local tensile strain, especially along the axis of the Zn-duo at the origin of the symmetry breaking. Hence the in-chain Zn-Te bonds along the Zn-duo are longer than those bridged perpendicular to the Zn-duo, assimilating with Zn-Te bonds bridged onto 1-Zn, in principle (see above). This results in CdTe:1Zn vibrating at a higher frequency than CdTe:2Zn. The whole picture symmetrically replicates at x~1 except that the local strain is inverted, resulting in four quasi parallel PM-TO branches $\{TO^{Zn}_{Cd-Te}, TO^{Cd}_{Cd-Te}, TO^{Zn}_{Zn-Te}, TO^{Cd}_{Zn-Te}\}$ tilted upward with increasing Zn content, from low to high frequency.

Straight PM-TO branches interpolated between the asymptotic *ab initio* (SIESTA) frequencies (at x~0,1) – which suffices to fix ideas – are compared in Fig. 4 (main panel) with experimental trends for the occasion grouped into three main branches (thin-plain curves, replicated from Fig. 1) – as recently suggested by Kozyrev[12] – likewise simplified to linearity for the sake of consistency. The experimental and *ab initio* pictures are globally consistent up to a slight frequency lag (~15 cm^{-1}) due to a well-known bias of the LDA to overestimate the bond force constants (**Sec. II.D**). The 1-Imp. and 2-Imp Γ-projected Ph-DOS are quasi degenerate in the Zn-dilute limit (x→0) and well-separated at large Zn content (x→1). Hence a distinct percolation-type fine structuring of the PM-TO modes is likely to be detected in a standard room temperature Raman/IR experiment on $Cd_{1-x}Zn_xTe$ (next **Sec.**) at large Zn content (x≥0.5). On reducing the Zn content, both the Cd-Te and the Zn-Te fine structures are expected to become more and more compact until merging into a unique feature at $x \to 0$, eventually leaving the impression of a crude MREI-like behavior from moderate Cd content onwards (x≤0.5).

Further AIMPRO *ab initio* insight into the Raman intensities is searched for at x=0.5 **(Sec. II**) by using a large (216-atom) $Cd_{54}Zn_{54}Te_{108}$ (50 at.% Cd) disordered zincblende supercell. This is needed to elucidate the sensitivity of bond vibrations to the local environment behind the percolation splitting – provided this can be visualized – as to whether this operates up to first (as for all studied III-V's so far) or second neighbors (the standard for II-VI's). This in turn governs the oscillator strength distribution between the two submodes within a percolation doublet, thus impacting their relative Raman intensities. For instance, at x~0.5 the Raman intensity ratio would be ~1:1 taking into account the effect of first neighbors only, and ~1:2 when accounting of the second neighbors as well.[32]

In fact, the Raman spectrum calculated *ab initio* by AIMPRO for the $Cd_{54}Zn_{54}Te_{108}$ supercell, shown in Fig. 4 (thin-dotted curve, x=0.5), reveals a mere MREI-like 2-mode pattern, without any clue of percolation-type fine structuring. Though the Cd-Te (lower) and Zn-Te (upper) Raman signals are well separated, the frequency gap between them (~30 cm^{-1}) exceeding the natural bandwidth due to inherent fluctuations in the local composition (roughly double), no fine structure is visible neither within the Cd-Te spectral range nor within the Zn-Te one. Probably this is because the large natural bandwidth (similar for Cd-Te and Zn-Te) screens the predicted (SIESTA) percolation splitting (~5 cm^{-1}, **Sec. A**). We have checked that the screening persists at large Zn content (Fig. S1) though the percolation splitting is presumably better resolved (Fig. 4).

The AIMPRO $Cd_{54}Zn_{54}Te_{108}$ PM-TO Raman spectrum is anyway useful to test the validity of our Raman cross section. We have checked (not shown) that fair contour modeling of the *ab initio* Raman lineshape is achieved via Eq. (1) – for the occasion compacted to two oscillators – with the used set of input parameters (**Sec. II.C.**). This gives confidence for modeling experimental data in the next Section.

Summarizing, the *ab initio*-SIESTA insight into the Raman frequencies via the Γ-projected Ph-DOS of our prototypical dual-impurity motif is conclusive in the positive sense for what regards the existence of distinct Cd-Te and Zn-Te percolation-type fine structures in the Cd-dilute limit ($x \to 1$), however, compacting into apparent (1-bond→1-mode) MREI-like patterns in the Zn-dilute limit ($x \to 0$). In fact, subsequent *ab initio*-AIMPRO calculations of the PM-TO Raman intensities fails to detect any fine structuring at intermediary composition (x=0.5), *i.e.*, where the alloy disorder achieves

maximum. This keeps us blocked from elucidating the sensitivity of bond vibrations to the local environment behind each doublet. More intensive *ab initio* calculations using larger supercells likely to improve the statistics on the alloy disorder and along with it the signal-to-noise ratio – falling beyond the scope of this work – would be needed to resolve any percolation-type fine structuring. In the next Section we alternatively resort to experiment – offering a naturally large statistics on the alloy disorder.

IV. EXPERIMENTAL (PM-TO, PP, LO) RAMAN STUDY OF $Cd_{1-x}Zn_xTe$

In this Sec., novel experimental $Cd_{1-x}Zn_xTe$ Raman insights are brought to attention aiming, first, to elucidate the sensitivity of bond vibrations to their local environment (as formalized in the percolation scheme), using PM-TO modes as the most relevant path (**Sec. IV.A.**), next, to investigate the PP's, so far left unexplored in ZnTe-based mixed crystals (**Sec. IV.B.**), and, last, to shed light onto persisting anomalies in the literature concerned with the LO modes (**Sec. IV.C.**).

A. Non-polar (PM-TO) modes

Unless forced into close proximity, the PM-TO modes hardly couple and thus preserve the natural phonon diversity of a mixed crystal,[6] as already mentioned.

As such they are well-suited to check *de visu* any percolation-type fine structuring in experimental $Cd_{1-x}Zn_xTe$ Raman spectra. The Raman study is placed at large Zn content, where the percolation splitting is presumably best-resolved based on the current *ab initio* predictions (Fig. 4) – hence putting a natural emphasis and Zn-environments – a pending issue at the term of our *ab initio* study (**Sec. III**).

A direct Raman insight into the $Cd_{1-x}Zn_xTe$ PM-TO modes at large Zn content is obtained in the backscattering geometry (corresponding to a maximum q-transfer and hence probing the native PM-TO regime of phonon-polaritons, **Sec. II-C**) at normal incidence/detection onto/from (110)-cleaved crystal faces (TO allowed, LO forbidden).

The study is done at low (77 K) temperature using the red (632.8 nm) laser excitation (with energy lying slightly underneath E_0 – see Fig. 3a). The temperature drop improves the quality of the first-order Raman signal, both directly, *i.e.*, by increasing the phonon lifetime (and hence decreasing the phonon damping), and also indirectly, *i.e.*, by ruining the two-phonon zone-edge band (abbreviated 2A) that emerges nearby (partly screening the zone-center Cd-Te Raman signal). The 2A band is further minimized by using crossed polarizations, adjusted to an angle that maximizes the PM-TO signal (marked ① in Fig. 5a). Though the LO modes are theoretically forbidden in the used geometry, significant contributions show up at any x values. These are presumably activated due to the nearly resonant excitation conditions – not sufficient to generate LO-harmonics though – that cannot be fully avoided whichever visible laser excitation is used (Fig. 3a).

The PM-TO modes are much sharper at 77K (Fig. 5b) than at room temperature (Fig. S2) – the FWHM of Raman peaks is reduced by more than half – revealing a distinct shoulder on the high-frequency tail of the dominant ZnTe-like signal. The shoulder does not proceed from any disorder-induced breaking of the wavevector conservation rule that governs the Raman scattering, leading to consider PM-TO contributions at finite q values besides the nominal q~0 one, because the ZnTe PM-TO mode is (slightly) dispersive towards low-frequency on departing from Γ, and not towards high-frequency.[9] We deduce, rather, that it is a genuine first-order Raman signal.

In fact, the shoulder has PM-TO symmetry since it obeys the same selection rules as the dominant ZnTe-like PM-TO of all studied $Cd_{1-x}Zn_xTe$ crystals. The theoretical Greek cross- (thick curves) and butterfly-like (thin curves) motifs in crossed and parallel polarizations of the incident and scattered lights are ideally replicated in experiment (symbols), not only with pure ZnTe (x=0, Figs. S2a and S2b) – which is already remarkable, but also at the maximum tested chemical disorder (x=0.87, Fig. 5a) – in the addressed composition domain corresponding to large Zn content, the sign of high vibrational and structural qualities.

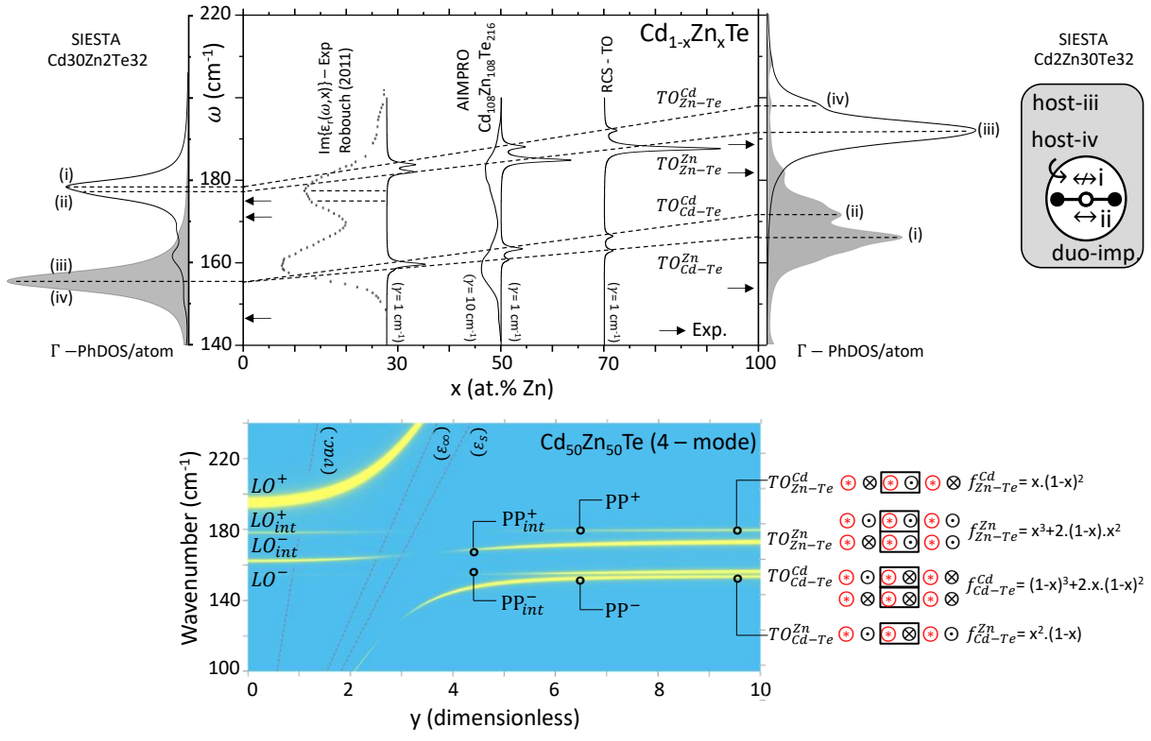

FIG. 4. $Cd_{1-x}Zn_xTe$ (PM-TO) percolation scheme fixed by *ab initio* calculations. *Ab initio* calculations revealing end (x~0,1) PM-TO frequencies of the four-mode $\{2\times(Cd-Te), 2\times(Zn-Te)\}$ $Cd_xZn_{1-x}Te$ percolation scheme obtained by applying the SIESTA code to a duo (forming a simple chain) of neighboring impurities immersed in a large (64-atom) supercell, as schematized at right. Labels (i) to (iv) therein refer to in-chain, out-of-chain, near-chain and away-from-chain vibration modes, in this order. The resulting Γ-PhDOS per Zn (clear surfaces) and Cd (shaded surfaces) atom flank the main panel (a) on both sides. The four $PM-TO$ branches are linearly interpolated between the limit parent and impurity duo-like frequencies (dashed lines). The (x~0,1)-ends of experimental $PM-TO$ branches (taken from Fig. 1) are indicated (using arrows), for comparison. The Raman spectrum obtained by applying the AIMPRO code to a large (216-atom) disordered $Cd_{0.5}Zn_{0.5}Te$ supercell (thick line) completes an *ab initio* insight into the Raman intensities at intermediary composition. The $Im\{\varepsilon_r(\omega, x=0.28)\}$ spectrum derived by Robouch *et al*. from IR-reflectivity measurements (digitalized from Ref. 37) – that assimilates with the $PM-TO$ Raman spectrum in a crude approximation – and the PM-TO Raman cross sections obtained at well-spanned x values (0.28, 0.5, 0.72) by operating Eq. (1) onto a four-mode $\{2\times(Cd-Te), 2\times(Zn-Te)\}$ description of $Cd_xZn_{1-x}Te$ assuming a sensitivity of bond vibrations up to second-neighbors are added (thin curves), for comparison. A minimal phonon damping (γ) is used (as specified) for clear resolution of neighboring features. The 1D-oscillator(s) behind each Raman peak are sketched out for clarity, specifying their fractions in the crystal (f-terms). An overview of the four-mode ($PM-TO$, LO, Phonon-polaritons – PP) Raman intensities/frequencies at x=0.5 obtained via Eq. (1) completes the picture (b).

More precisely, we have no example of the shoulder surviving the inhibition of the main PM-TO feature or inversely (examples of raw polarized Raman data are given in Figs. S2a and S2d).

In view of all this, the detected shoulder at large Zn content is identified as a genuine first-order q~0 feature with PM-TO symmetry, intrinsic to alloying. The shoulder reinforces with the Cd content and is slightly blue-shifted with respect to the dominant ZnTe-like PM-TO signal. As such, it meets all requirements for being assigned as TO^{Cd}_{Zn-Te} (Fig. 4), in which case the main ZnTe-like feature is re-assigned as TO^{Zn}_{Zn-Te}. Hence, the ZnTe-like PM-TO Raman signal is bimodal, of percolation-type and not of MREI-type.

Fair contour modeling of the raw $Cd_{0.13}Zn_{0.87}Te$ PM-TO Raman signal – taken as a case study – is achieved in Fig. 5 (thick curve) by applying the relevant version of our Raman cross section (RCS) given in Eq. (1) –

corresponding to the divergence of $\varepsilon_r(\omega, x)$ – to a three-PM-TO

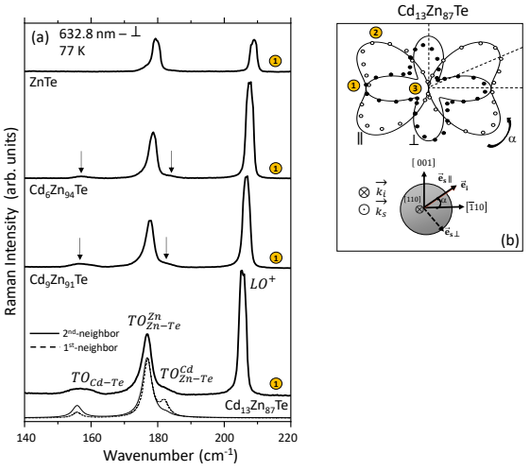

FIG. 5. $Cd_{1-x}Zn_xTe$ Raman $PMTO$–symmetry analysis at large Zn content. (a) Polarized $Cd_{13}Zn_{87}Te$ $PMTO$-like Raman spectra taken at 77 K in the backscattering geometry onto (110)-cleaved crystal faces using the 632.8 nm laser line. (b) The variations of Raman intensity of the dominant Zn-Te signal measured at the same sample spot depending on the azimuth α (as sketched out) in crossed (⊥, filled symbols) and parallel (∥, empty symbols) polarizations are superimposed onto the corresponding theoretical greekcross- and butterfly-like patterns, for comparison. The Raman intensities (normalized to the maximum value in each series) match over a complete α-revolution (360°) of the (⊥,∥)-paired polarizations at the sample surface. The critical α angle maximizing the PM-TO signal in crossed (⊥) polarizations – needed to switch off the spurious 2A band (see text) – used to record the various Raman spectra in panel (a) is symbolized ①. Similar critical α angles maximizing – ② – and switching off – ③ – the PM-TO signals in parallel (∥) polarizations – used in Fig. S5 – are also indicated.

$\{TO_{Cd-Te}, TO^{Zn}_{Zn-Te}, TO^{Cd}_{Zn-Te}\}$ description. A sensitivity of Zn-Te vibrations up to second neighbors is assumed. Two 1D-oscillators, due to the pure-Zn and mixed-(Cd,Zn) local environments, come under TO^{Zn}_{Zn-Te}, while TO^{Cd}_{Zn-Te} relates to the remaining pure-Cd environment, as sketched out in Fig. 4. The fractions of related 1D-oscillators scale accordingly, specified by the f-terms as indicated. The only used alloy-related input parameters are the PM-TO frequencies and the full widths at half maximum (FWHM) of Raman peaks, directly taken from experiment. A similar simulation done by limiting the sensitivity to first-neighbors (Fig. 5, dashed curve), added for the sake of completeness, fails to mimic the intensity balance between the two Zn-Te submodes.

Similar (second-neighbor) theoretical $Cd_{1-x}Zn_xTe$ Raman lineshapes (thin curves) now expanded into the full four-PMTO $\{TO^{Zn}_{Cd-Te}, TO^{Cd}_{Cd-Te}, TO^{Zn}_{Zn-Te}, TO^{Cd}_{Zn-Te}\}$ description obtained at well-spanned x values (~0.3, 0.5, ~0.7) by linearly interpolating the PM-TO frequencies between their parent- and impurity-like *ab initio* values (Fig. 4, dashed curves) and by taking a minimal phonon damping (1 cm^{-1}) for a clear resolution of neighboring features are shown in Fig. 4. The dominance of TO^{Zn}_{Zn-Te} over TO^{Cd}_{Zn-Te} apparent in experiment at large Zn content (x=0.87, Fig. 5) persists up to intermediate composition (x=0.50) until reversal of the intensity balance on crossing the critical composition x~0.30. The trend is symmetric for Cd-Te. In fact, the high-resolution IR data for x=0.28 collected at a synchrotron by Robouch *et al.*[37] transformed into proper $Im\{\varepsilon_r(\omega, x)\}$ spectra (assimilating with PM-TO Raman spectra in a crude approximation) by applying the Kramers-Krönig transformation to raw data, reproduced in our Fig. 4 (dotted curve), actually demonstrates the onset of reversal (arrows), consistently with RCS predictions.

To complete such snapshots at selected x-values, we show (Fig. S6) how the available Zn-Te oscillator strength divides between the two percolation-type Zn-Te submodes when x varies, depending on whether the Zn-Te vibrations "feel" the local environment up to first- (thin lines) or second neighbors (thick lines). Corresponding Raman and IR data at large Zn content (this work, open symbols) and at small-moderate Zn content (Kozyrev,[12] filled symbols) are added for comparison. Only the hypothesis of non-negligible sensitivity to the nature of second-neighbors withstands the comparison with experiment. As such, $Cd_{1-x}Zn_xTe$ deviates from $Zn_{1-x}Be_x$-chalcogenides, in which the sensitivity to first neighbors is dominant and sufficient. This explains the "abnormal" nature of $Cd_{1-x}Zn_xTe$ pointed out by Kozyrev[12] – issue 3.

In Fig. 5, the comparison between the experimental and theoretical $Cd_{0.2}Zn_{0.8}Te$ Raman spectra calculated on the basis of a unique Cd-Te feature is not very good in the Cd-

Te spectral range, suggesting an existence of some fine structure (an additional mode seems to emerge besides the main one, as indicated by an arrow). This nicely resonates with *ab initio* (Siesta) predictions at large Zn content. However, the experimental PM-TO signal is far too weak to decide in favor of a (percolation) fine structuring of the Cd-Te signal.

B. Polar (phonon-polariton, LO) modes

Further experimental TO insight into the (minor) CdTe-like signal at large Zn content is searched for hereafter (**Sec. B.1**) by shifting the Raman analysis from the PM-TO phonon regime to the phonon-polariton regime. This is needed in view to achieve a consistent TO picture prior to addressing the LO modes further on (**Sec. B.2**).

1. Phonon-polaritons at large Zn content (300 K)

Fig. 6 displays the theoretical q-dependent phonon-polariton Raman spectra of $Cd_{0.09}Zn_{0.91}Te$ – taken as a case study – obtained by operating the relevant version (ε_r=q^2c^2/ω^2) of the RCS given by Eq. (1) onto a compact three-oscillator $\{1\times(Cd-Te), 2\times(Zn-Te)\}$ description (**Sec. A**) – consistent with experiment – reflecting a sensitivity of Zn-Te vibrations up to second neighbors.

Both the phonon-polariton dispersion (curves) and the Raman intensities (thickness of curves) are delivered. A minimal phonon damping (1 cm^{-1}) is adopted for clarity.
The only used alloy-related input parameters are the experimental PM-TO frequencies (Fig. 6, referring to the Raman signal that flanks the main panel at the right).

By shifting the Raman study from 77 K (Fig. 5) to room temperature (Fig. 6), all Raman features are softened by a few cm^{-1} – due to a strengthening of chemical bonds – and broadened (by more than half), so that the minor TO^{Cd}_{Zn-Te} now merely generates a slight asymmetry on the high frequency tail of the dominant TO^{Zn}_{Zn-Te}. Corresponding near-forward Raman spectra, taken at the same sample spot at near-normal incidence of the near-infrared (785.0 nm) at the rear of the crystal so as to achieve various minimal scattering angles, flank the main panel at the left.

A brief description of the theoretical phonon-polariton Raman spectra (main panel) is useful to fix ideas prior to a discussion of experimental data.

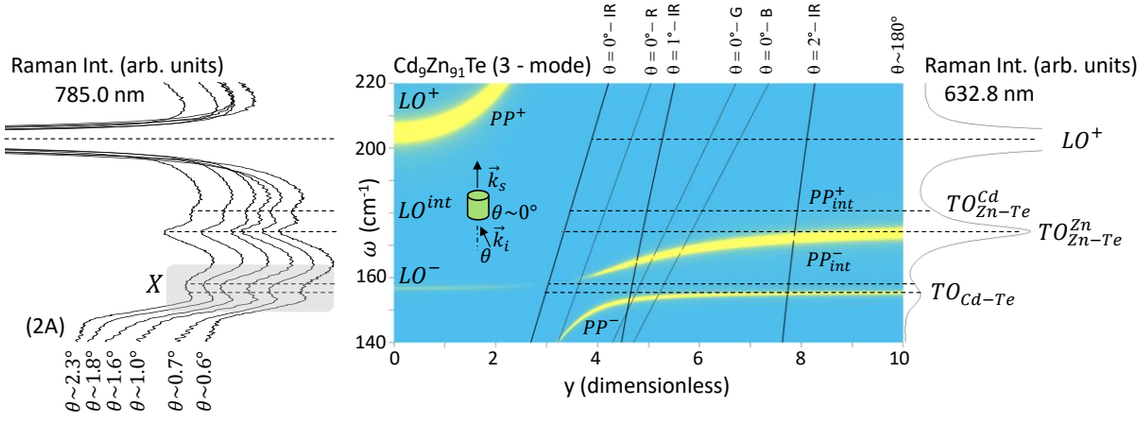

FIG. 6. $Cd_{1-x}Zn_xTe$ PP–coupling at large Zn content. Theoretical dispersion (curves) and Raman intensity (thickness of curves) of the $Cd_{0.13}Zn_{0.87}Te$ phonon-polaritons calculated via Eq. (1) within a simplified three-mode $[1\times(Cd-Te), 2\times(Zn-Te)]$ version of the $Cd_xZn_{1-x}Te$ percolation scheme (main panel). The Raman scan lines derived (from the wavevector conservation law) in the nearly perfect forward scattering geometry (θ=0°, 1°,2°) via the dispersion of the refractive index (Fig. 3b) measured close to the near-infrared (IR, 785.0 nm), red (R, 632.8 nm), green (G, 514.5 nm) and/or blue (B, 488.0 nm) laser lines are superimposed to visualize which phonon-polaritons are accessible experimentally. $Cd_{0.08}Zn_{0.12}Te$ near-forward Raman spectra taken with the 785.0 nm laser line at various small scattering angles θ (as indicated) flank the main panel at left. The sensitive Cd-Te spectral range is emphasized (shaded area). The corresponding backward Raman spectrum taken at the same sample spot with the 632.8 nm laser line – used for reference purpose – flanks the main panel at right. Related Raman features in both geometries are connected (dotted lines)

$Cd_{0.09}Zn_{0.91}Te$ exhibits a negative $\omega(q)$ dispersion towards Γ ($q \to 0$), with two parent-like branches in repulsion (PP_- and PP_+) framing two alloy-related S-like branches (PP_{int}^- and PP_{int}^+). The parent- and alloy-like phonon-polaritons differ in nature in view of their asymptotic regimes close to Γ and away from it, being differently governed by a pair of (photon, phonon) asymptotes and by a pair of phonon asymptotes, respectively. On crossing the photon regime near the S-inflexion, the alloy-related phonon-polaritons are hardly supported by the lattice and transiently suffer a total Raman collapse (referred to as the photon extinction hereafter), conforming to intuition that only matter-like elementary excitations scatter light efficiently.

The Raman intensities are further impacted by the coupling that develops between neighboring TO modes via their transverse photon-like electric field E_T as soon as they engage their phonon-polariton regime. $Cd_{1-x}Zn_xTe$ is a model system in this respect due to the compacity of the native PM-TO phonons behind the phonon-polaritons. Generally, the E_T-coupling (transverse symmetry) channels the available oscillator strength towards low frequency – and not towards high-frequency as with the E_L-coupling,[32] the reason why PP_{int}^+ is hardly visible and PP_{int}^- so strong in Fig. 6. The E_T-coupling achieves maximum in the sensitive bottleneck region where PP_{int}^- (stemming from the dominant $PM - TO_{Zn-Te}^{Zn}$) softens down to PP_- (that proceeds from the minor $PM - TO_{Cd-Te}$), just before diverging and catching up with their respective LO_- and photon-like asymptotes near Γ (q=0). In the bottleneck the E_T-coupling generates a massive $PP_{int}^- \to PP_-$ transfer of oscillator strength, to such extent that PP_- transiently dominates over PP_{int}^- on the verge of collapse by assimilation with its lower photon asymptote.

The experimental detection of the transient PP_{int}^- reinforcement regime is a real challenge. To anticipate which laser line is best suited, various "Raman scan lines" $\omega(q)$ corresponding to different laser excitations and scattering angles $\theta = \left(\widehat{\vec{k}_i, \vec{k}_s}\right)$ inside the crystal – depending on the used Raman scattering geometry via the wavevector conservation law ($\vec{k}_i - \vec{k}_s = \vec{q}$) – are superimposed (oblique lines) onto the $Cd_{0.09}Zn_{0.91}Te$ phonon-polariton dispersion (Fig. 6). The detected phonon-polaritons in a given Raman experiment lie at intersection between the phonon-polariton dispersion and the relevant Raman scan line for the used scattering geometry.

More precisely, at a given scattering angle θ the magnitude q of the transferred wavevector depends on the laser excitation via the dispersion of the refractive index nearby (currently accessed by ellipsometry – Fig. 3b). Hence, a Raman scan line is both laser- and θ -dependent. Among the various laser lines at hand (785nm – near-IR, 632.8 nm – red, 514.5 nm – green, 488.0 nm – blue), the more energetic green and blue laser lines are absorbed by the crystal (Fig. 3a) and thus irrelevant for near-forward Raman measurements. Even if extremely thin crystal slices – sufficient to offer a path through the crystal in spite of the strong absorption – were used, both laser lines would anyway fall short of addressing the sensitive bottleneck zone; only the asymptotic PM-TO regime is within their reach due to the large dispersion of the refractive index that increases on approach of the optical band gap (Fig. 3b). As for the red laser line, given the minimal achievable scattering angle in practice, *i.e.*, $\theta \sim 1°$ in this case, it can merely probe the early stage of the phonon-polariton regime away from Γ (on departing from the native PM-TO modes). In fact, only the near-IR laser line, falling in the "blind" zone (of the photon-like extinction) at zero scattering angle (not achievable experimentally – see above) is likely to address the bottleneck, where all phonon-polaritons are subject to rapid metamorphosis – referring notably to the transient PP_- enhancement on the verge to collapse onto its photon-like asymptote. However, for doing so, θ should not exceed a few degrees at most (Fig. 6).

In practice the near-forward θ-dependent Raman spectra taken at room temperature with pure ZnTe at (quasi) normal incidence/detection throughout parallel (110)-cleaved crystal faces using the red laser line (Fig. S3a) give only access to the early phonon-polariton still "attached to" its native $PM -$

TO_{Zn-Te} feature, whichever scattering angle is used. Several attempts to "detach" the phonon-polariton – by varying the incidence of the incoming red laser beam and/or by using the near-IR laser line – remained unsuccessful. It is as if the Zn-Te phonon-polariton hardly survives (and becomes overdamped, *i.e.*, not observable) as soon as departing from its native PM-TO phonon, for some reason. This we have to keep in mind for $Cd_{1-x}Zn_xTe$.

When shifting from backscattering (right panel, Fig. 6) to near-forward scattering using the red laser line, only the Zn-Te signal is reactive, in the same way as observed with ZnTe (Fig. S3b). The situation improves by changing to the near-IR laser excitation (left panel, Fig. 6), in that both the Zn-Te and Cd-Te signals are reactive.

The dominant ZnTe-like PM-TO suffers a dramatic collapse (down to the level of the 2A bands nearby, the latter bands being yet so minor that they are hardly observed in backscattering – right panel), the sign that the deep phonon-polariton regime is engaged. The reminiscent $PM-TO_{Zn-Te}^{Zn}$ in the forward Raman spectra is an allowed feature generated in backscattering by the incident laser beam on its way back towards the rear crystal face after reflection at the front crystal face. Note that in this scattering geometry the $PM-TO_{Zn-Te}^{Cd}$ shoulder, being degenerated with LO^{int}, is clearly resolved, providing further experimental (PP-like) evidence for the Zn-Te splitting. This is a side effect of the multiple reflections of the laser beam between both crystal faces to massively enhance the theoretically forbidden LO modes[70] – presently ascertained by the strong LO^{+} emergence.

Now, we turn to the minor Cd-Te signal, of central interest. As ideally expected, the CdTe-like phonon-polariton is detected in the sensitive bottleneck region, *i.e.*, in the form of a distinct X feature (left panel) that progressively softens on the verge of collapse into its photon-like dispersive regime (shaded area). Moreover, a slight enhancement is transiently observed, conforming to predictions. However, a disconcerting feature is that the softening develops above $PM-TO_{Cd-Te}$, by as much as ~5 cm^{-1}, and not below it. Given the experimentally achievable (*q,y*)-values (bounded by the $\theta = 0°$ near-IR Raman scan line at minimum), no phonon-polariton is likely to show up in this spectral range within the current three-mode $\{1\times(Cd-Te), 2\times(Zn-Te)\}$ description retained for $Cd_{1-x}Zn_xTe$ (Fig. 6). The discussed anomaly can be explained only if the native Cd-Te PM-TO behind the detected phonon-polariton is not unique, *i.e.*, MREI-like – as considered in Fig. 6 in a crude approximation – but actually double, *i.e.*, of the percolation type. Hence, the current experiment points towards a canonical four-mode $\{TO_{Cd-Te}^{Zn}, TO_{Cd-Te}^{Cd}, TO_{Zn-Te}^{Zn}, TO_{Zn-Te}^{Cd}\}$ percolation scheme for $Cd_{1-x}Zn_xTe$, consistently with *ab initio* (Siesta) predictions, solving issue 4.

In fact the $Cd_{1-x}Zn_xTe$ phonon-polariton dispersion derived on such four-mode basis assuming a sensitivity of Cd-Te vibrations to second neighbors (by analogy with Zn-Te) provides an additional phonon-polariton PP_{int}^{-} due to TO_{Cd-Te}^{Cd} that slightly softens above the main $PP\_$ one (asymptotically attached to TO_{Cd-Te}^{Zn}) at quasi stable Raman intensity – consistently with experimental observations – before eventually collapsing on approach to its photon-like extinction. The as-simulated (*q,y*)-dependent phonon-polariton Raman signal at the representative composition x=0.5 shown in Fig. 4b is illustrative in this respect. Only $PP\_$ is clearly enhanced on receipt of the Zn-Te oscillator strength due to $\vec{E}_T$-coupling with the dominant ZnTe-like mode (PP_{int}), when this latter, descending in its S-like dispersion towards Γ, is forced to proximity with both Cd-Te oscillator(s). PP_{int}^{-} merely acts as a mediator in this transfer, with quasi no impact on its Raman intensity which hardly suffers any disruption in the process. As for the upper ZnTe-like PP_{int}^{+} feature that carries negligible amount of oscillator strength, it plays a minor role. Yet, $PP\_$ is not observed experimentally, presumably due to its immediate collapse into a destructive interference with the 2A-continuum lying flush with PM-TO_{Cd-Te}^{Zn} (Fig. 6 – left) as soon as the latter mode softens on engaging its phonon-polariton regime. Retrospectively, such collapse is a major boon that facilitates the detection of PP_{int}^{-} (Fig. 4), remaining as a decisive experimental evidence

for the bimodal character of the Cd-Te Raman signal.

2. LO modes at small to moderate Zn content (77 K)

Now we turn to LO modes and tackle two pending issues in the $Cd_{1-x}Zn_xTe$ Raman data (Fig. S4), namely that the Zn-Te impurity mode (x~0) shows up as strongly as the Cd-Te lattice one (located at a slightly lower frequency)[14,23,25] – issue 1, and that the latter mode rapidly collapses to zero as soon as departing from the Zn-dilute limit[26] – issue 2. Both features are intrinsic to $Cd_{1-x}Zn_xTe$-alloying (**Sec. I**), hence deserving an explanation.

The E_L-coupling between neighboring LO modes via their common macroscopic electric field E_L provides a suitable framework for the discussion of such apparent anomalies, because this coupling's main effect is to channel the available oscillator strength towards high frequency (**Sec. I**).[31] Applied to $Cd_{1-x}Zn_xTe$, this is expected to emphasize the upper Zn-Te mode (recipient of oscillator strength) – issue 1 – at the expense of the lower (donor) Cd-Te one – issue 2, at any x value.

At small to moderate Zn content, most of the available oscillator strength is awarded to the second oscillator in the canonical four-mode $\{(Cd-Te)^{Zn}, (Cd-Te)^{Cd}, (Zn-Te)^{Zn}, (Zn-Te)^{Cd}\}$ percolation series – in which notation the superscript refers to the local environment of a vibrating bond (specified in brackets). Being in fact the impurity modes, the three other oscillators are almost deprived of oscillator strength. Yet, the upper two LO modes need a priori to be considered on top of the main one (related to the second oscillator), because the three LO modes in question emerge at close frequencies and hence subject to strong E_L-coupling. As for the lowest oscillator, being both minor and off-resonant, it can be omitted in the first approximation. This suggests a three-mode $\{Cd-Te, (Zn-Te)^{Zn}, (Zn-Te)^{Cd}\}$ description combining a MREI behavior for Cd-Te together with a percolation one for Zn-Te. Hence, an intra-bond $(Zn-Te)^{Zn} \rightarrow (Zn-Te)^{Cd}$ E_L-coupling has to be taken into account on top of the inter-bond $(Cd-Te) \rightarrow (Zn-Te)$ one, in principle.

A crude insight into the main inter-bond E_L-coupling at x~0 is achieved by adopting a crude two-mode $\{1\times(Cd-Te), 1\times(Zn-Te)\}$ MREI-like description, in which the two close minor recipient Zn-Te sub-modes are artificially compacted into a single feature for the sake of clarity. In doing so, we replicate the approach used by Groenen *et al.*[15] in a similar context with $In_{1-x}Ga_xAs$ (**Sec. I**). The intra-bond E_L-coupling will be discussed at a later stage, for the sake of completeness.

By omitting the phonon damping, useless in the cited approach, the mechanical equations characterizing each oscillator write as $\mu_i\left[\omega_{T,i}^2(x)-\omega^2\right]u_i = Z_iE$, materializing the E-coupling between oscillators with i=1, 2 standing for Cd-Te and Zn-Te, respectively. Considering that $\varepsilon_r(\omega,x)=0$ for LO modes, a relation emerges between E – then equipped with the relevant L subscript – and (u_1,u_2), used to re-formulate the equations of motion into a self-consistent system of two (u_1,u_2)-coupled oscillators. Introducing the normal coordinates $Q_i=\sqrt{Nx_i\mu_i}$ and assuming that the dynamical charge (Z_i) does not depend on the composition x,[33] the coupled system takes the form

$$\begin{pmatrix} E_1(x)-\omega^2 & V(x) \\ V(x) & E_2(x)-\omega^2 \end{pmatrix}\begin{pmatrix} Q_1 \\ Q_2 \end{pmatrix} = \tilde{0}, \qquad (3)$$

involving the off-diagonal coupling term $V(x)=\sqrt{x\times(1-x)}\times\varepsilon_\infty^{-1}(x)\times E_{12}$ – with $E_{12}=\Omega_1\times\Omega_2\times\sqrt{\varepsilon_{\infty1}\times\varepsilon_{\infty2}}$ (with Ω defined in Sec. II.C) – together with the diagonal eigenfrequencies of the raw/uncoupled LOs given by $E_i(x)=\omega_{Ti}^2(x)+x_i\times\varepsilon_{\infty i}\times\varepsilon_\infty^{-1}(x)\times\Omega_i^2$, with x_i referring to the fraction of the i-bond species in the crystal and keeping the conventional meaning for the used symbols (**Sec. II**). Solving the secular equation gives access to the eigenfrequencies of the coupled-$LO^{\pm}$ modes, *i.e.*,

$$\omega_\pm^2(x)=\left(\frac{E_1(x)+E_2(x)}{2}\right)\pm\sqrt{\Delta(x)^2+V(x)^2}, \qquad (4)$$

depending on the strength of the coupling $V(x)$ and on the proximity $\Delta(x) = \frac{E_2(x)-E_1(x)}{2}$ with the resonance between the raw-uncoupled LOs. In fact, the $\omega_{\pm}^2(x)$ eigenvalues were already accessible as by-products of the LO Raman cross section. On the other hand, the related unit eigenvectors,

$$|Q_{\pm}\rangle = \left(\frac{1}{\sqrt{V^2(x)+\left(\mp\Delta(x)+\sqrt{\Delta^2(x)+V^2(x)}\right)^2}}\right) \times \begin{pmatrix} \mp\Delta(x)+\sqrt{\Delta^2(x)+V^2(x)} \\ \pm V(x) \end{pmatrix}, \quad (5)$$

are useful to assess how much (in percent) a given bond (Cd-Te or Zn-Te) is involved in a given coupled-$LO^{\pm}$ mode, as captured via the $cos^2\theta$ and $sin^2\theta$ terms within the convenient sine and cosine notation of $|Q_+\rangle = \begin{pmatrix} cos\,\theta \\ sin\,\theta \end{pmatrix}$ and $|Q_-\rangle = \begin{pmatrix} -sin\,\theta \\ cos\,\theta \end{pmatrix}$, being clear that $|Q_{\pm}\rangle$ are orthogonal at any x value. In this case, $\tau = \tan\theta$ represents the degree of mixing between Q_1 and Q_2 in each coupled-$LO^{\pm}$ mode. Besides, $\sin 2\theta = -V(x)/\sqrt{\Delta^2(x)+V^2(x)}$ and $\cos 2\theta = \Delta(x)/\sqrt{\Delta^2(x)+V^2(x)}$, introducing $|\tan 2\theta| = V(x)/\Delta(x)$ as a convenient measure of the net efficiency of the E_L −coupling in terms of a compromise between the strength of the coupling and the proximity with the resonance (of the bare uncoupled-LO modes).

Direct insights into the x-dependence of such parameters for $Cd_{1-x}Zn_xTe$ (solid lines) are given in Fig. 7. Similar curves obtained for $In_{1-x}Ga_xAs$ – replicating those originally produced by Groenen *et al.*[15] – are added (dashed lines), for comparison.

In the absence of coupling ($V = 0$), $cos^2\theta = 1$ while $sin^2\theta$ and τ become 0, meaning that the upper and lower LO modes selectively involve the Zn-Te and Cd-Te vibrations at any x value, respectively.

The inter-bond coupling takes effect in $Cd_{1-x}Zn_xTe$ and $In_{1-x}Ga_xAs$ already from high dilution of the short/stiff bond due to a combination of quasi resonant condition ($\Delta \to 0$) and large coupling (V, reaching half its maximum value already from ~5 at.% impurity content).

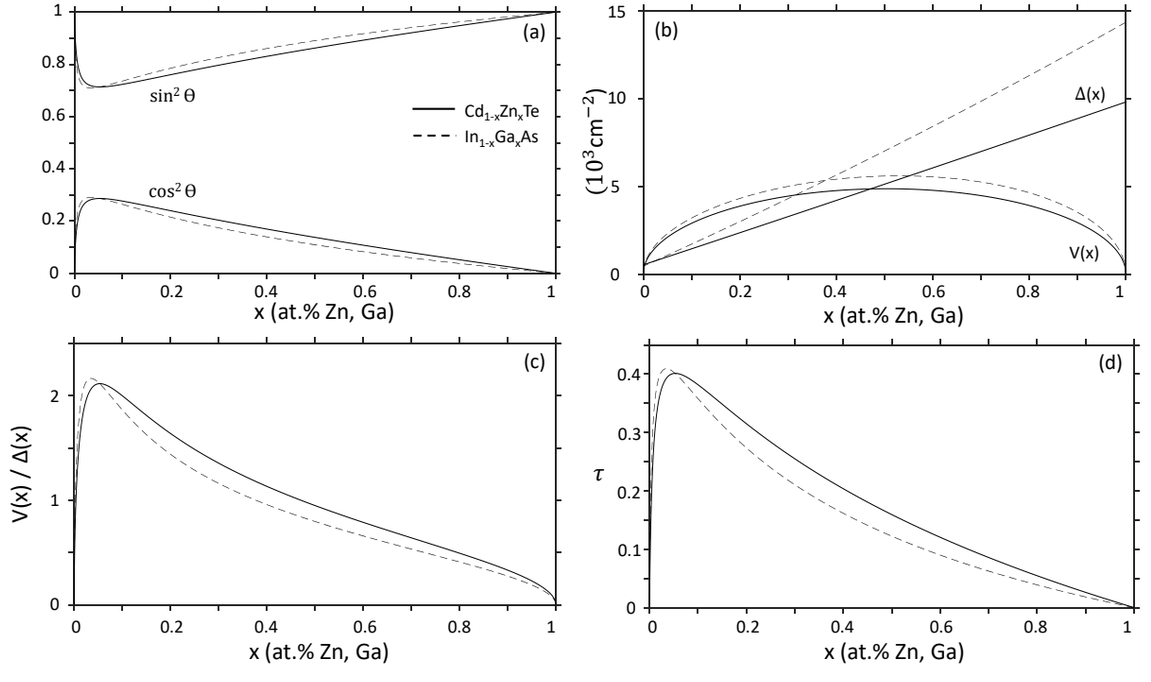

FIG. 7. $Cd_{1-x}Zn_xTe$ MREI-like LO–coupling. Composition dependence of parameters characterizing the E_L-coupling in $Cd_{1-x}Zn_xTe$ ultimately simplified to a two-mode $[1 \times (Cd-Te), 1 \times (Zn-Te)]$ MREI-like description (solid lines), *i.e.*, $cos^2\theta$ and $sin^2\theta$ (a), $\Delta(x)$ and $V(x)$ (b), $V(x)/\Delta(x)$ (c) and τ (d). Corresponding curves for $In_{1-x}Ga_xAs$ are added (dashed lines), for comparison.

This generates a strong inter-mode mixing at this limit (testified by pronounced deviations of $cos^2\theta$ and $sin^2\theta$ from 1 and 0, respectively), the reason why the Zn-Te mode emerges so strongly in the Raman spectra – issue 1. The resonance is progressively detuned on departing from the Zn-dilute limit, however compensated by a gradual reinforcement of the coupling (which achieves maximum at x~0.5). Hence the E_L –coupling remains strong up to intermediate composition. The net effect is to dramatically favor the upper LO_+ at the expense of the lower LO_-. This explains the fast collapse of the latter feature from minor Zn incorporation onwards – issue 2, subsequently relayed by the natural disappearance of LO_- on entering the Cd-poor domain – the CdTe-like oscillator strength becoming negligible then. Altogether this leaves the impression of an overall 1-LO mode behavior across (most of) the composition domain. Fig. 8a reporting the 2-mode $\{1\times(Cd-Te),(1\times(Zn-Te)\}$ $Cd_{1-x}Zn_xTe$ LO Raman cross section in its composition dependence is illustrative in this respect. In contrast, two distinct LO modes remain visible at any x value with $In_{1-x}Ga_xAs$, as apparent in Fig. 8b, testifying for a stronger E_L –coupling for the $Cd_{1-x}Zn_xTe$ II-VI mixed crystal than for the twin III-V $In_{1-x}Ga_xAs$ one.

To fully appreciate how much the coupled (LO_-, LO_+) $Cd_{1-x}Zn_xTe$ Raman spectra (experimental) are distorted with respect to the raw-uncoupled (LO_{Cd-Te}, LO_{Zn-Te}) ones (theoretical), we have calculated via Eq. (1) equipped with the relevant condition on $\varepsilon_r(\omega,x)$ – specified within brackets – the two corresponding series of theoretical LO ($\varepsilon_r=0$) Raman lineshapes at well-spanned x values, further considering the underlying PM-TO ($\varepsilon_r\to\infty$) Raman signals, for reference purpose. The only used alloy-related input parameters are the PM-TO frequencies – best adjusted from experiment as quadratic x-dependencies (Fig. 1, solid lines). Technically, the uncoupled LO modes – labeled as the native PM-TO modes – were obtained by artificially truncating $\varepsilon_r(\omega,x)$ to the sole oscillator of interest in the Raman cross section.

By expanding $\varepsilon_r(\omega,x)$ to two oscillators, the E_L-coupling is activated, which truly shakes the LO Raman signal regarding both the Raman frequencies and the Raman intensities. A comparative insight into the x-dependencies of the normalized optical bandwidths $\delta_p(x)=\left[\omega_{L,p}^2(x)-\omega_{T,p}^2(x)\right]/\omega_{T,p}^2(x)$ *per* p-oscillator (a) and of the LO_-/LO_+ Raman intensity ratio (b), with (solid-thin lines) and without (dashed lines) E_L-coupling, is given in Fig. 9. Basically, the upper/lower mode gains/loses oscillator strength due to the strong E_L-coupling at small to moderate Zn content, with concomitant impact on the optical bandwidth and on the Raman intensity of the Zn-Te/Cd-Te modes, being increased/reduced with respect to the uncoupled case.

A deeper insight into $\delta_p(x)$ is achieved by comparing the theoretical two-mode trends shown in Fig. 9a (solid-thin lines) with $\delta_p(x)$ values directly derived from the abundant TO and LO CdTe- and ZnTe-like frequencies measured across the composition domain by Granger *et al.*[38] using IR-reflectivity (symbols).

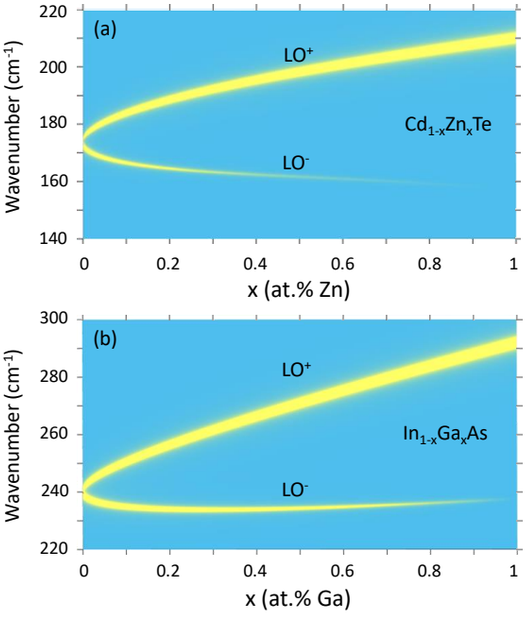

FIG. 8. $Cd_{1-x}Zn_xTe$ vs. $In_{1-x}Ga_xAs$ MREI-like LO Raman signals. (a) Theoretical coupled-LO Raman spectra of $Cd_{1-x}Zn_xTe$ calculated via Eq. 1 by assuming a crude two-mode $\{1\times(Cd-Te),1\times(Zn-Te)\}$ MREI description at minimal phonon damping (1 cm^{-1}), covering both the Raman frequencies (curves) and the Raman intensities (thickness of curves). The corresponding spectra for $In_{1-x}Ga_xAs$ are added (b), for comparison.

The experimental Zn-Te and Cd-Te data slightly overestimate the theoretical ones, respectively, at any x value. This is at least partly due to the percolation-type fine structuring of the Zn-Te signal, that artificially emphasizes the TO-LO splitting. In fact, the proximity with experiment is improved when considering the novel theoretical data set obtained within the more refined three-mode $\{1\times(Cd-Te),2\times(Zn-Te)\}$ description of $Cd_{1-x}Zn_xTe$ (solid-thick lines) – in line with Figs. 1 (PM-TO frequencies) and 4 (f-terms), and identifying $\omega_{T,Zn-Te}(x)$ with the frequency of the lower and generally dominant TO^{Zn}_{Zn-Te} feature. The 2-mode picture remains, however, valid in its main lines.

We have checked (Fig. S7) that the 2-mode MREI-like picture for the LOs of $Cd_{1-x}Zn_xTe$ is not challenged by adopting the complete 4-mode $\{2\times(Cd-Te),2\times(Zn-Te)\}$ picture. This is because the intra-bond E_L-coupling is (quasi) total within both compact Cd-Te and Zn-Te doublets. Fig. S7 further reveals that the intra-bond (Zn-Te) coupling is quasi-resonant with the inter-bond one in $Cd_{1-x}Zn_xTe$, a side effect of the Zn-Te sensitivity up to second neighbors. In contrast, the intra-bond (Ga-As) E_L –coupling is detuned from the inter-bond one with the twin $In_{1-x}Ga_xAs$ system,[3] a side effect of the Ga-As sensitivity limited to first-neighbors.

Due to the tuning/detuning of the intra- and inter-bond couplings in $Cd_{1-x}Zn_xTe/In_{1-x}Ga_xAs$ described in terms of 3-mode systems, one may be tempted to consider that the coupling is more efficient for $Cd_{1-x}Zn_xTe$ than for $In_{1-x}Ga_xAs$, the reason why $Cd_{1-x}Zn_xTe$ would exhibit an apparent 1-LO behavior throughout most of the composition domain and not a 2-LO one as $In_{1-x}Ga_xAs$. However, this is a wrong track since the MREI- like (2-mode) description suffices *per se* to explain such discrepancy (Fig. 8).

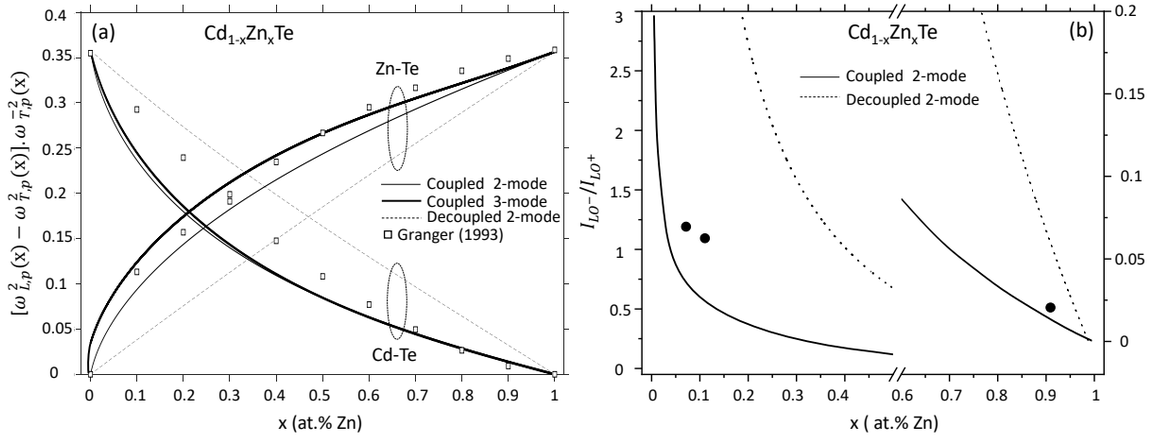

FIG. 9. $Cd_{1-x}Zn_xTe$ – optical bandwidths and Raman intensities. Theoretical (plain lines) composition dependencies of the normalized optical bandwidths (a) and of the intensity interplay between the upper (+) and lower (-) LO Raman features within the crude two-mode $\{1\times(Cd-Te),1\times(Zn-Te)\}$ MREI-type description of $Cd_{1-x}Zn_xTe$ (solid-thin curves) and its more refined three-mode $\{1\times(Cd-Te),2\times(Zn-Te)\}$ percolation-type variant (solid thick curves) – in line with Figs. 1 (frequency aspect) and 4 (f-terms). Well-documented IR experimental data taken from the literature (empty symbols, a) and the current Raman ones (solid symbols, b) are superimposed, for comparison.

V. CONCLUSION

This work reports on an exhaustive experimental backward/near-forward Raman study of all possible Raman-active modes (TOs, LOs, phonon-polaritons) of $Cd_{1-x}Zn_xTe$ single crystals of high purity and high structural quality (verified by X-ray diffraction), grown by using the Bridgman method across the composition domain, with *ab initio* (SIESTA and AIMPRO) calculations in support. Ellipsometry measurements are further needed to access the dispersion of the refractive index in the visible coming as a major ingredient in the Raman cross section of phonon-polaritons.

$Cd_{1-x}Zn_xTe$ exhibits a multifaceted Raman behavior generally falling into the scope of our percolation scheme but taking a number of forms depending on the composition domain and on the phonon symmetry as well. At large Cd-content, the $Cd_{1-x}Zn_xTe$ phonon behavior fits into a basic two-mode $\{1\times(Cd-Te), 1\times(Zn-Te)\}$ MREI scheme, whereas a more accurate percolation-type description is required at large Zn content. The canonical four-mode $\{2\times(Cd-Te), 2\times(Zn-Te)\}$ percolation pattern becomes, however, apparent when exploring the phonon-polariton (polar-TO) regime. Yet, a crude three-mode $\{1\times(Cd-Te), 2\times(Zn-Te)\}$ version suffices to capture the native purely-mechanical (non polar) TOs behind the phonon-polaritons. The phonon behavior ultimately simplifies into a unique/compact $\{1\times(Cd-Te, Zn-Te)\}$-mixed-mode in the LO symmetry – formalized as a MREI sub-case – due to a coupling between neighboring LOs via their long-range electric field.

Comparing eigenvectors, the LO-coupling appears to be stronger in the current II-VI $Cd_{1-x}Zn_xTe$ mixed crystal than in the twin III-V $In_{1-x}Ga_xAs$ one, in fact characterized by two distinct LOs across the composition domain. Further, the sensitivity of bond vibrations to the local environment behind the bimodal percolation-type fine structuring of Raman signals is limited to first neighbors for $In_{1-x}Ga_xAs$ whereas it extends up to second neighbors for $Cd_{1-x}Zn_xTe$.

Retrospectively, *i.e.*, in view of all re-examined systems so far – in which the assignment of the upper (best-resolved) percolation doublet was supported by a careful contour modeling of raw experimental Raman data (specified in brackets below) – the difference in sensitivity of bond vibrations to the local environment evidenced in $In_{1-x}Ga_xAs$ (first neighbors) and $Cd_{1-x}Zn_xTe$ (second neighbors) emerges as a rule throughout III-Vs ($Ga_{1-x}In_xAs$ – Ref. 3, $Ga_{1-x}In_xP$ – Ref. 71, $GaAs_{1-x}P_x$ – Ref. 72) and II-VIs ($Cd_{1-x}Zn_xSe$ – Ref. 57, $ZnS_{1-x}Se_x$ – Ref. 32, $Cd_{1-x}Zn_xTe$ – this work) – with II-VI $Zn_{1-x}Be_x$-chalcogenides standing out as the only exception (Refs. 73, 74).

As formulated, the short/long-range sensitivity of III-V/II-VI bond vibrations to the local environment in mixed crystals seems intimately related to their covalent/ionic character – the II-VI Be-bonding assimilating with III-Vs in this respect.[1] Generally, such basic (yet so far unsuspected) distinction between the phonon mode behaviors of II-VI and III-V semiconductor mixed crystals – to be further tested/verified – is interesting on the fundamental side.

The current formalization of the bimodal Raman pattern per bond of $Cd_{1-x}Zn_xTe$ within the percolation scheme is also interesting with respect to applications. In particular, it offers the possibility to achieve a quantitative / fast / non-destructive insight into the nature of the Cd↔Zn atom substitution at a given composition by comparing the Raman intensities of the two (non polar) TO submodes forming the best-resolved (Zn-Te) percolation doublet at this composition. Depending on whether such Raman intensity ratio matches, underestimates or overestimates the ratio between the corresponding f^{Cd}_{Zn-Te} and f^{Zn}_{Zn-Te} oscillator fractions (as specified in Fig. 4), one may conclude that the Cd↔Zn substitution is ideally random or reflects a trend towards local clustering or anticlustering, correspondingly. Such analysis has earlier been conducteed with, *e.g.*, $Cd_xZn_{1-x}Se$ – Ref. 57 and $Ge_{1-x}Si_x$ – Ref. 75.

SUPPLEMENTARY MATERIAL

Additional insights into the phonon mode behavior of $Cd_{1-x}Zn_xTe$ covering the PM-TOs (symmetry analysis, *ab initio* – AIMPRO – calculations of Raman spectra), preliminary phonon-polariton Raman studies (using the red – 632.8 nm laser line) and the LOs (refined to a three-mode description) – in this order, are reported as supplementary material.

ACKNOWLEDGEMENTS

We acknowledge assistance from the PSICHÉ beamline staff of synchrotron SOLEIL (Proposal 20210410 – standard, BAG for PSICHÉ beamline led by Y.L.G., sub-project-HP-CdZnTe co-led by A.P. & O.P.), from the IJL core facility (Université de Lorraine – http://ijl.univ-lorraine.fr/recherche/centres-de-competences/rayons-x-et-spectroscopie-moessbauer-x-gamma) for the X-ray diffraction measurements and from the Ellipsometry platform of LCP-A2MC (Université de Lorraine – http://lcp-a2mc.univ-lorraine.fr). The *ab initio* SIESTA calculations have been done using the facilities of the EXPLOR mesocentre of the Université de Lorraine (project 2019CPMXX0918). VJBT acknowledge the FCT through projects LA/P/0037/2020, UIDB/50025/2020 and UIDP/50025/2020.

AUTHOR DECLARATION

Conflict of Interest
The authors have no conflict to disclose.

Author Contributions

T. Alhaddad: Data curation; Formal analysis; Investigation; Software; Validation; Visualization. **M. B. Shoker:** Data curation; Formal analysis; Software; Validation. **O.Pagès:** Conceptualization; Funding acquisition (lead); Methodology; Project administration (lead); Supervision (lead); Writing original draft (lead). **A. V. Postnikov:** Formal analysis, Funding acquisition (supporting); Project administration (supporting); Software; Writing original draft (supporting). **V. J. B. Torres:** Formal analysis, Funding acquisition (supporting); Software. **A. Polian:** Investigation; Project administration (supporting); Supervision (supporting); Writing original draft (supporting). **Y. Le Godec:** Resources. **J.-P. Itié:** Investigation ; Project administration (supporting). **L. Broch:** Investigation. **M. B. Bouzourâa:** Investigation. **A. En Naciri:** Investigation. **S. Diliberto:** Investigation. **S. Michel:** Investigation. **P. Franchetti:** Investigation. **A. Marasek:** Resources. **K. Strzałkowski:** Resources ; Project administration (supporting).

DATA AVAILABILITY

The data that support the findings of this study are available from the corresponding author upon reasonable request.

REFERENCES

[1] C. Vérié, « Beryllium substitution-mediated covelency engineering of II-VI alloys for lattice elasticity reinforcement," J. Cryst. Growth **184 /185**, 1061 (1998).

[2] M. T. Man, Y. Yu and H. S. Lee, "Energy separation and carrier-phonon scattering in CdZnTe/ZnTe quantum dots on Si subtsrate," J. Alloys and Compounds **658**, 71 (2016)

[3] O. Pagès, T. Tite, K. Kim, P. A. Graf, O. Maksimov and M. C. Tamargo, "Percolation picture for long wave phonons in zinc-blende mixed crystals: from (Zn,Be)-chalcogenides to (Ga,In)As," J. Phys. Condens. Matter **18**, 577 (2006).

[4] I. F. Chand and S. S. Mitra, "Application of a modified random-element-isodisplacement model to long-wavelength optic phonons of mixed crystals," Phys. Rev. **172**, 924 (1968).

[5] H. Verleur and A. S. Jr. Barker, "Infrared Lattice vibrations in $GaAs_yP_{1-y}$ alloys," Phys. Rev. **149**, 715 (1966).

[6] M. B. Shoker, T. Alhaddad, O. Pagès, V. J. B. Torres, A. V. Postnikov, A. Polian, R. Hajj Hussein, G.K. Pradhan, C. Narayana, C. Gardiennet, G. Kervern, L. Nataf, S. Ravy, J.-P. Itié, K. Strzałkowski, A. Marasek and F. Firszt, "Exceptional phonon point versus free phonon coupling in $Zn_{1-x}Be_xTe$ under pressure: an experimental and *ab initio* Raman study," Sci. Rep. **12**, 753 (2022).

[7] W. Weber, "New bond charge model for the lattice dynamics of diamond-type semiconductors," Phys. Rev. Lett. **33**, 371 (1974).

[8] K. C. Rustagi and W. Weber, "Adiabatic bond charge model for the phonons in A^3B^5 semiconductors," Solid State Commun. **18**, 673 (1976).

[9] B. D. Rajput and D. A. Browne, "Lattice dynamics of II-VI materials using the adiabatic bond-charge model," Phys. Rev. B **53**, 9052 (1996).

[10] M. B. Shoker, O. Pagès, V. J. B. Torres, A. Polian, J.-P. Itié, G.K. Pradhan, C. Narayana, M. N. Rao, R. Rao, C. Gardiennet, G. Kervern, K. Strzałkowski, and F. Firszt, "Phonon-based partition of (ZnSe-like) semiconductor mixed crystals on approach to their pressure-induced structural transition," Sci. Rep. **10**, 19803 (2020).

[11] A. A. Wronkowska, H. Arwin, F. Firszt, S. Łęgowski, A. Wronkowski and Ł. Skowroński, "Optical spectra of $Zn_{1-x}Be_xTe$ mixed crystals determined by IR-VIS-UV ellipsometry and photoluminescence measurements," Thin Solid Films **519**, 2795 (2011).

[12] S. P. Kozyrev, "Features of the percolation scheme of transformation of the vibrational spectrum with varying alloy composition for Cd(TeSe) and (CdZn)Te alloys with soft bonds," Semiconductors **49**, 885 (2015).

[13] N. E. Christensen, S. Satpathy and Z. Pawlowska, "Bonding and ionicity in semiconductors," Phys. Rev. B **36**, 1032 (1987).

[14] D. J. Olego, P. M. Raccah and J. P. Faurie, "Compositional dependence of the Raman frequencies and line shape of $Cd_{1-x}Zn_xTe$ determined with films grown by molecular beam epitaxy," Phys. Rev. B **33**, 3819 (1986).

[15] J. Groenen, R. Carles, G. Landa, C. Guerret-Piécourt, C. Fontaine and M. Gendry, "Optical-phonon behavior in $Ga_{1-x}In_xAs$: the role of microscopic strains and ionic plasmon coupling," Phys. Rev. B **58**, 10452 (1998).

[16] J. L. Martins and A. Zunger, "Bond lengths around isovalent impurities and in semiconductor solid solutions," Phys. Rev. B **30**, 6217 (1984).

[17] Y. Cai and M. F. Thorpe, "Length mismatch in random semiconductor alloys. II. Structural characterization of pseudobinaries," Phys. Rev. B **46**, 15879 (1992).

[18] D. Zamir, K. Beshah, P. Becla, P. A. Wolf, R. G. Griffin, D. Zax, S. Vega and N. Yellin, "Nuclear magnetic resonance studies of II-VI semiconductor alloys," J. Vac. Sci. technol. A **6**, 2612 (1988).

[19] R. D. Feldman, R. F. Austin, A. H. Dayem and E. H. Westerwick, "Growth of

$Cd_{1-x}Zn_xTe$ by molecular beam epitaxy," Appl. Phys. Lett. **49**, 797 (1986).

[20] R. J. Elliott, J. A. Krumhansl and P. L. Leath, "The theory and properties of randomly disordered crystals and related physical systems," Rev. Modern Phys. **46**, 465 (1974).

[21] D. W. Taylor, in Optical properties of mixed crystals, edited by R. J. Elliott and I. P. Ipatova (Elsevier, North-Holland, 1988), Chap.2, p. 78.

[22] S. Adachi, Properties of Semiconductor Alloys: Group-IV, III-V and II-VI Semiconductors (John Wiley & Sons, Inc., Chichester, 2009), Chap. 4, p. 110.

[23] D. N. Talwar, Z. C. Feng and P. Becla, "Impurity-induced phonon disordering in $Cd_{1-x}Zn_xTe$ ternary alloys," Phys. Rev. B **48**, 17067 (1993).

[24] O. Castaing, R. Granger, J. T. Benhlal and R. Triboulet, "The dielectric function and interband transitions in $Cd_{1-x}Zn_xTe$," J. Phys. Condens. Matter **8**, 5757 (1996).

[25] P. D. Paulson, B. E. McCandless, and R. W. Bikmire, "Optical properties of $Cd_{1-x}Zn_xTe$ films in a device structure using variable angle spectroscopic ellipsometry," J. Appl. Phys. **95**, 3010 (2004).

[26] S. Perkowitz, L. S. Kim, Z. C. Feng and P. Becla, "Optical phonons in $Cd_{1-x}Zn_xTe$," Phys. Rev. B **42**, 1455 (1990).

[27] A. Aydinli, A. Compaan, G. Contreras-Puente and A. Mason, "Polycristalline $Cd_{1-x}Zn_xTe$ thin films grown on glass by pulsed laser deposition," Solid State Commun. **80**, 465 (1991).

[28] D. N. Talwar, Z. C. Feng, J.-F.Lee and P. Becla, "Extended x-ray absorption fine structure and micro-Raman spectra of Bridgman grown $Cd_{1-x}Zn_xTe$ ternary alloys," Materials Research Express **1**, 015018 (2014).

[29] Y.V. Znamenshchykov, V. V. Kosyak, A. S. Opanasyuk, V. O. Dorda, P. M. Focuk and A. Medvids, "Raman characterization of $Cd_{1-x}Zn_xTe$ thick polycrystalline films obtained by the close-spaced sublimation," Acta Physica Polonica A **132**, 1430 (2017).

[30] D. N. Talwar, P. Becla, H.-H. Lin and Z. C. Feng, "Assessment of intrinsic and doped defects in Bridgman grown $Cd_{1-x}Zn_xTe$ alloys," Mat. Sci. Eng. B **269**, 115160 (2021).

[31] J. Geurts, "Analysis of band bending at III-V semiconductor interfaces by Raman spectroscopy," Surface Science reports **18**, 1 (1993).

[32] R. Hajj Hussein, O. Pagès, S. Doyen-Schuler, H. Dicko, A. V. Postnikov, F. Firszt, A. Marasek, W. Paszkowicz, A. Maillard, L. Broch and O. Gorochov, "Percolation-type multi-phonon pattern of Zn(S,Se): backward/forward Raman scattering and *ab initio* calculations," J. Alloys and Compounds **644**, 704 (2015).

[33] H. Harada and S.-I. Narita, "Lattice vibrations of $Zn_xCd_{1-x}Te$ alloys," J. Phys. Soc. Japan **30**, 1628 (1971).

[34] J. J. Polit, E. M. Sheregii, E. Burattini, A. Marcelli, M. Cestelli Guidi, P. Calvani, A. Nucara, M. Piccinini, A. Kisiel, J. Konior, E. Sciesiński and A. Mycielski, "Analysis of phonon spectra of the $Zn_xCd_{1-x}Te$ solid-solution," J. Alloys and Compounds **371**, 172 (2004).

[35] T.-Z. Yang, S.H. Jhang, Y.-H. Shih, F.-C. Hou, Y.-C. Yang, P. Becla, D.-C. Tien and Z. C. Feng, "Far-IR reflectance spectra analysis of CdZnTe and related materials," Proc. of SPIE **7449**, 74490L (2009).

[36] S. P. Kozyrev, V. N. Pyrkov and L. K. Vodopyanov, "Vibrational-spectrum rearrangement of $Cd_{1-x}Zn_xTe$ semiconductor alloys," Fizika Tverdogo Tela **34**, 2367 (1992).

[37] B. V. Robouch, I. V. Kutcherenko, M. C. Guidi, A. Kisiel, A. Marcelli, P. Robouch, M. Piccinini, A. Nacura, R. Triboulet, E. Burattini, J. Cebulski, E. M. Sheregii and J. Polit, "Ion distribution preferences in ternary crystals $Zn_xCd_{1-x}Te$, $Zn_{1-x}Hg_xTe$ and $Cd_{1-x}Hg_xTe$," Eur. Phys. J. B **84**, 183 (2011).

[38] R. Granger, Y. Marqueton and R. Triboulet, "Optical phonons in bulk $Cd_{1-x}Zn_xTe$ mixed crystals in the whole composition range," J. Phys. I France **3**, 135 (1993).

[39] A. I. Belogorokhov, L. I. Belogorokhova, A. G. Belov, V. M. Lakeenkov, L. M. Liberant and N. A. Smirnova, "Atomic configuration and far-infrared optical spectra of lattice vibrations of Zn-Te and Cd-Te modes in $Cd_{1-x}Zn_xTe$ (x=0-0.2)," J. Cryst. Growth **159**, 186 (1996).

[40] P. R. Briddon and R. Jones, "LDA calculations using a basis of Gaussian orbitals," Phys. Stat. Sol. B **217**, 131 (2000).

[41] M. J. Rayson and P. R. Briddon, "Rapid iterative method for electronic-structure eigenproblems using localized basis functions," Comput. Phys. Commun. **178**, 128 (2008).

[42] J. M. Soler, E. Artacho, J. D. Gale, A. García, J. Junquera, P. Ordejón and D. Sánchez-Portal, "The SIESTA method for *ab initio* order-N materials simulation," J. Phys.: Condens. Matter **14**, 2745 (2002).

[43] D. T. Hon and W. L. Faust, "Dielectric parametrization of Raman lineshapes for GaP with a plasma of charge carriers," Appl. Phys. **1**, 241 (1973).

[44] K. Strzałkowski, "The composition effect on the thermal and optical properties across the CdZnTe crystals," J. Phys. D: Appl. Phys. **49**, 435106 (2016).

[45] D. T. F. Marple, "Refractive index of ZnSe, ZnTe and CdTe," J. Appl. Phys. **35**, 539 (1964).

[46] K. Sato and S. Adachi, "optical properties of ZnTe," J. Appl. Phys. **73**, 926 (1993).

[47] D. A. G. von Bruggeman, "Berechnung verschiedener physikalischer konstanten von heterogenen substanzen," Annal. der Physik **5**, 636 (1935).

[48] H. H. Li, "Refractive index of ZnS, Znse, and ZnTe and its wavelength and temperature derivative," J. Phys. Chem. Ref. Data **13**, 103 (1984).

[49] Handbook of Ellipsometry, edited by H. G. Tompkins and E. A. Irene (Willian Andrew, publishing, Springer, Norwich, 2005), Chaps. 2 & 3.

[50] H. Dicko, O. Pagès, F. Firszt, K. Strzałkowski, W.Paszkowicz, A. Maillard, C. Jobard and L. Broch, "Near-forward Raman selection rules for the phonon-polaritons in (Zn,Be)Se alloys," J. Appl. Phys. **120**, 185702 (2016).

[51] C. A. Arguello, D.L. Rousseau and S.P.S. Porto, "First-order Raman effect in wurtzite-type crystals," Phys. Rev. **181**, 1351 (1969).

[52] R. Hajj Hussein, O. Pagès, F. Firszt, W. Paszkowicz and A. Maillard, "Near-forward Raman scattering and bulk surface phonon-polaritons in the model percolation-type ZnBeSe alloy," Appl. Phys. Lett. **103**, 071912 (2013).

[53] V. C. Stergiou, A. G. Kontos, and Y. S. Raptis, "Anharmonic effects and Faust-Henry coefficient of CdTe in the vicinity of the energy gap," Phys. Rev. B **77**, 235201 (2008).

[54] M. Cardona, in Light Scattering in Solids II vol. **60**, edited by M. Cardona and G. Günterhodt (Springer, Berlin, 1982), p. 62.

[55] A. V. Postnikov, O. Pagès and J. Hugel, "Lattice dynamics of the mixed semiconductor (Be,Zn)Se from first-principles calculations," Phys. Rev. B **71**, 115206 (2005).

[56] N. Troullier and J. L. Martins, "Efficient pseudopotentials for plane-wave calculations," Phys. Rev. B **43**, 1993 (1991).

[57] M. B. Shoker, O. Pagès, H. Dicko, V. J. B. Torres, A. V. Postnikov, A. Polian, F. Firszt, K. Strzałkowski, A. En Naciri, L. Broch, M.N. Rao, R. Rao, A. Maillard and J.-P. Itié, "Multi-phonon (percolation) behavior and local clustering of $Cd_{1-x}Zn_xSe$-cubic mixed crystals ($x \leq 0.3$): A raman-*ab initio* study," J. Appl. Phys. **126**, 105707 (2019).

[58] J. P. Perdew and Y. Wang, "Accurate and simple analytic representation of the electron-gas correlation energy," Phys. Rev. B **45**, 13244 (1992).

[59] C. Hartwigsen, S. Goedecker, and J. Hutter, "Relativistic separable dual-space Gaussian pseudopotentials from H to Rn," Phys. Rev. B **58**, 3641 (1998).

[60] H. J. Monkhorst and J. D. Pack, "Special points for Brillouin-zone integrations," Phys. Rev. B **13**, 5188 (1976).

[61] F. Birch, "Finite elastic strain of cubic crystals," Phys. Rev. **71**, 809 (1947).

[62] I. Broser, R. Broser , H. Finkenrath , R. R. Galazka , H.E.Gumlich , A.Hoffmann, J. Kossut, E.Mollwo, H. Nelkowski , G. Nimtz , W. von der Osten, M. Rosenzweig , H.J. Schulz , D. Theis , D. Tschierse and O. Madelung (E.), in Physics of II-VI and I-VII Compounds, Semimagnetic Semiconductors, Landolt- Börnstein New series Group III, Vol. 17, Pt b, Springer, Berlin, 1982.

[63] O. Madelung, M. Schulz and H. Weiss, in Numerical Data and Functional Relationships in Science and Technology, Landolt-Börnstein (Eds.), vol. **17**, Springer, Berlin, 1982.

[64] J.-C. Li, L.-S. Li and W. Sun, "Temperature dependence on dielectric properties of CdTe and ZnTe using first-principles method and experimental data," Procedia Computer Science **174**, 673 (2020).

[65] E. Deligoz, K. Colakoglu and Y. Ciftci, "Elastic, electronic, and lattice dynamical properties of CdS, CdSe, and CdTe," Physica B **373**, 124 (2006).

[66] S. de Gironcoli, « Phonons in Si-Ge systems : An *ab initio* interatomic-force-constant approach," Phys. Rev. B **46**, 2412 (1992).

[67] P. R. Briddon and R. Jones, "LDA calculations using a basis of Gaussian orbitals," Phys. Status Solidi B **217**, 131 (2000).

[68] N. Vagelatos, D. Wehe, and J. S. King, "Phonon dispersion and phonon densities of states for ZnS and ZnTe," J. Chem. Phys. **60**, 3613 (1974).

[69] J.M. Rowe, R.M. Nicklow, D.L. Price and K. Zanio, "Lattice dynamics of cadmium telluride," Phys. Rev. B **10**, 671 (1974).

[70] C. H. Henry and J. J. Hopfield, "Raman scattering by polaritons," Phys. Rev. Lett. **15**, 964 (1965).

[71] O. Pagès, A. Chafi, D. Fristot and A. V. Postnikov, "(Ga,In)P: A standard alloy in the classification of phonon mode behavior," Phys. Rev. B **73**, 165206 (2006).

[72] O. Pagès, J. Souhabi, A. V. Postnikov and A. Chafi, "Percolation versus cluster models for multimode vibration spectra of mixed crystals: GaAsP as a case study," Phys. Rev. B **80**, 035204 (2009).

[73] O. Pagès, M. Ajjoun, T. Tite, D. Bormann, E. Tournié and K. C. Rustagi, "Long-wave phonons in ZnSe-BeSe mixed crystals: Raman scattering and percolation model," Phys. Rev. B **70**, 155319 (2004).

[74] O. Pagès, T. Tite, A. Chafi, D. Bormann, O. Maksimov and M. C. Tamargo, "Raman study of the random ZnTe-BeTe mixed crystal: Percolation model plus multimode decomposition," J. Appl. Phys. **99**, 063507 (2006).

[75] V. J. B. Torres, R. Hajj Hussein, O. Pagès and M. J. Rayson, "Clustering / anticlustering effects on the GeSi Raman spectra at moderate (Ge,Si) contents: Percolation scheme vs. *ab initio* calculations," J. Appl. Phys. **121**, 085704 (2017).

AIP Publishing

Journal of Applied Physics

ACCEPTED MANUSCRIPT

This is the author's peer reviewed, accepted manuscript. However, the online version of record will be different from this version once it has been copyedited and typeset.
PLEASE CITE THIS ARTICLE AS DOI: 10.1063/5.0134454

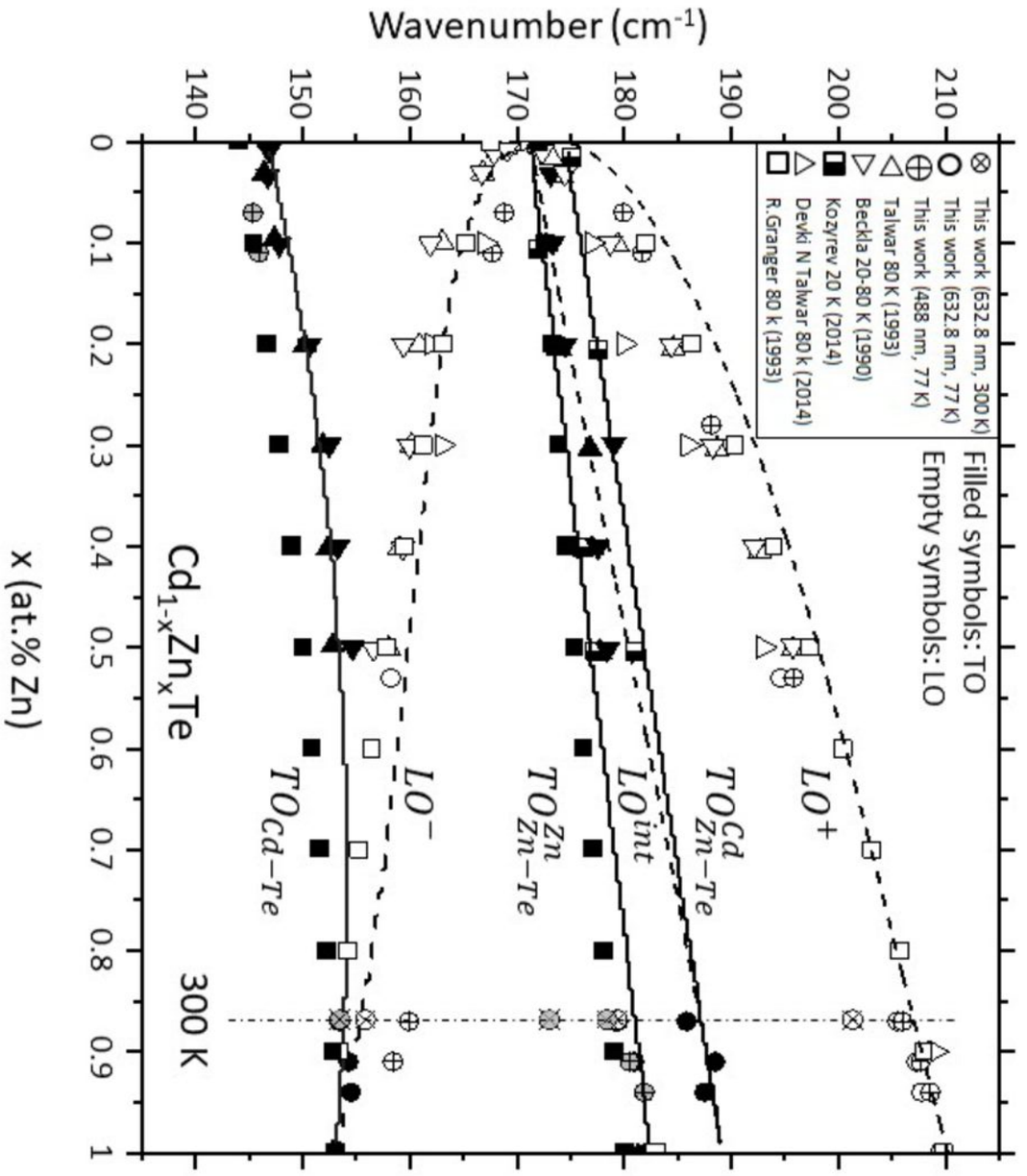

AIP Publishing

Journal of Applied Physics

ACCEPTED MANUSCRIPT

This is the author's peer reviewed, accepted manuscript. However, the online version of record will be different from this version once it has been copyedited and typeset.
PLEASE CITE THIS ARTICLE AS DOI: 10.1063/5.0134454

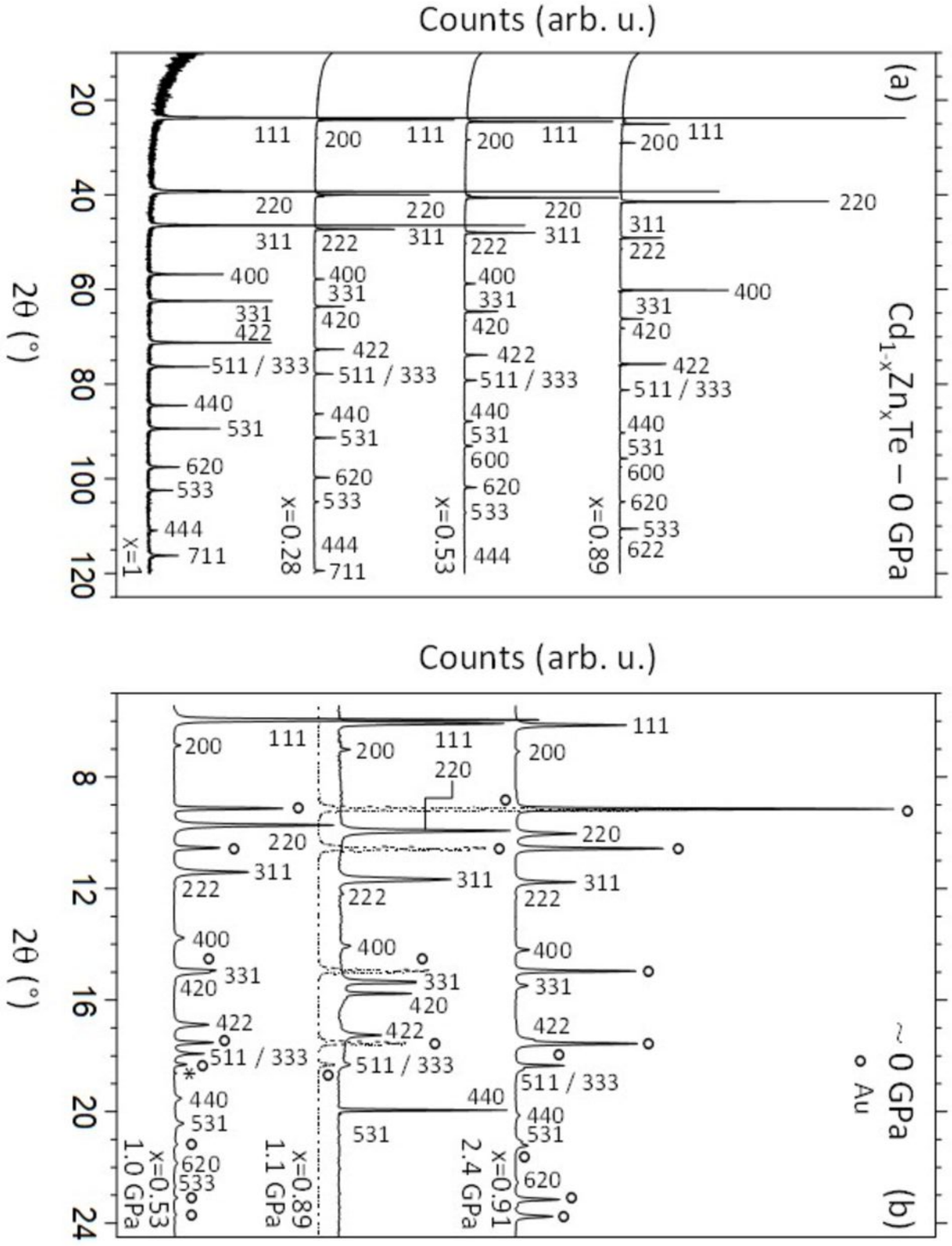

AIP Publishing

Journal of Applied Physics

ACCEPTED MANUSCRIPT

This is the author's peer reviewed, accepted manuscript. However, the online version of record will be different from this version once it has been copyedited and typeset.
PLEASE CITE THIS ARTICLE AS DOI: 10.1063/5.0134454

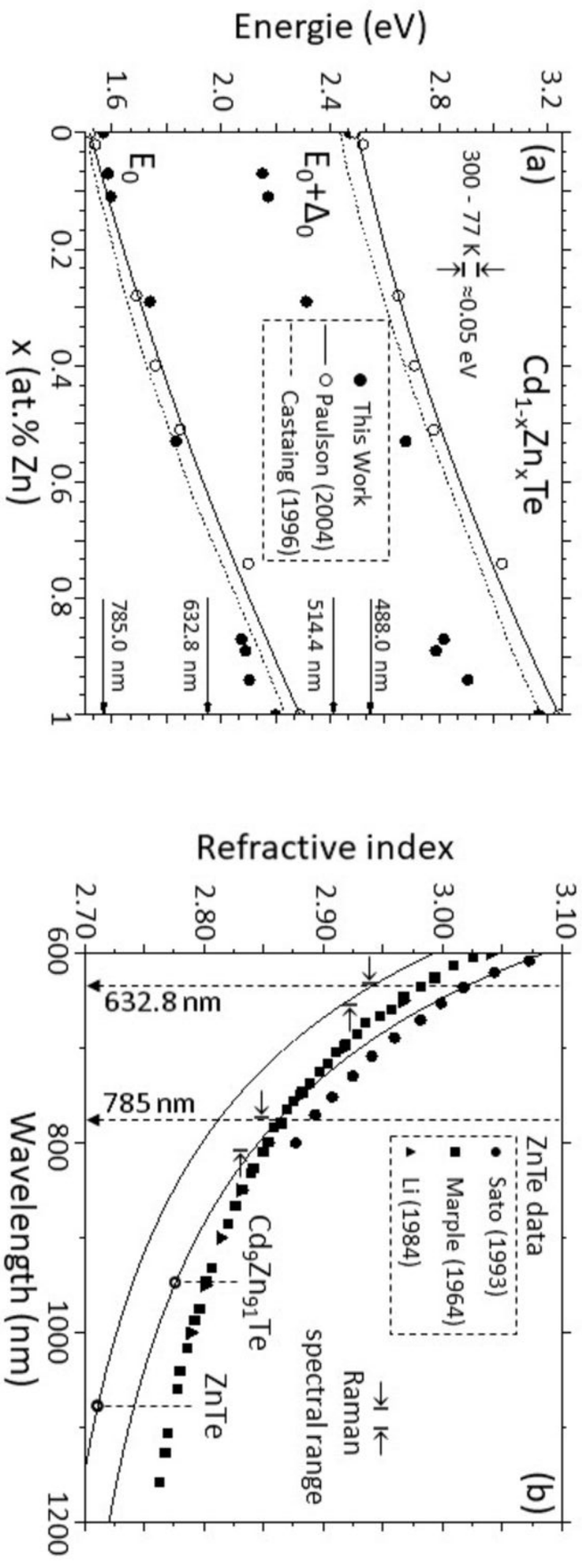

AIP Publishing

Journal of Applied Physics

ACCEPTED MANUSCRIPT

This is the author's peer reviewed, accepted manuscript. However, the online version of record will be different from this version once it has been copyedited and typeset.
PLEASE CITE THIS ARTICLE AS DOI: 10.1063/5.0134454

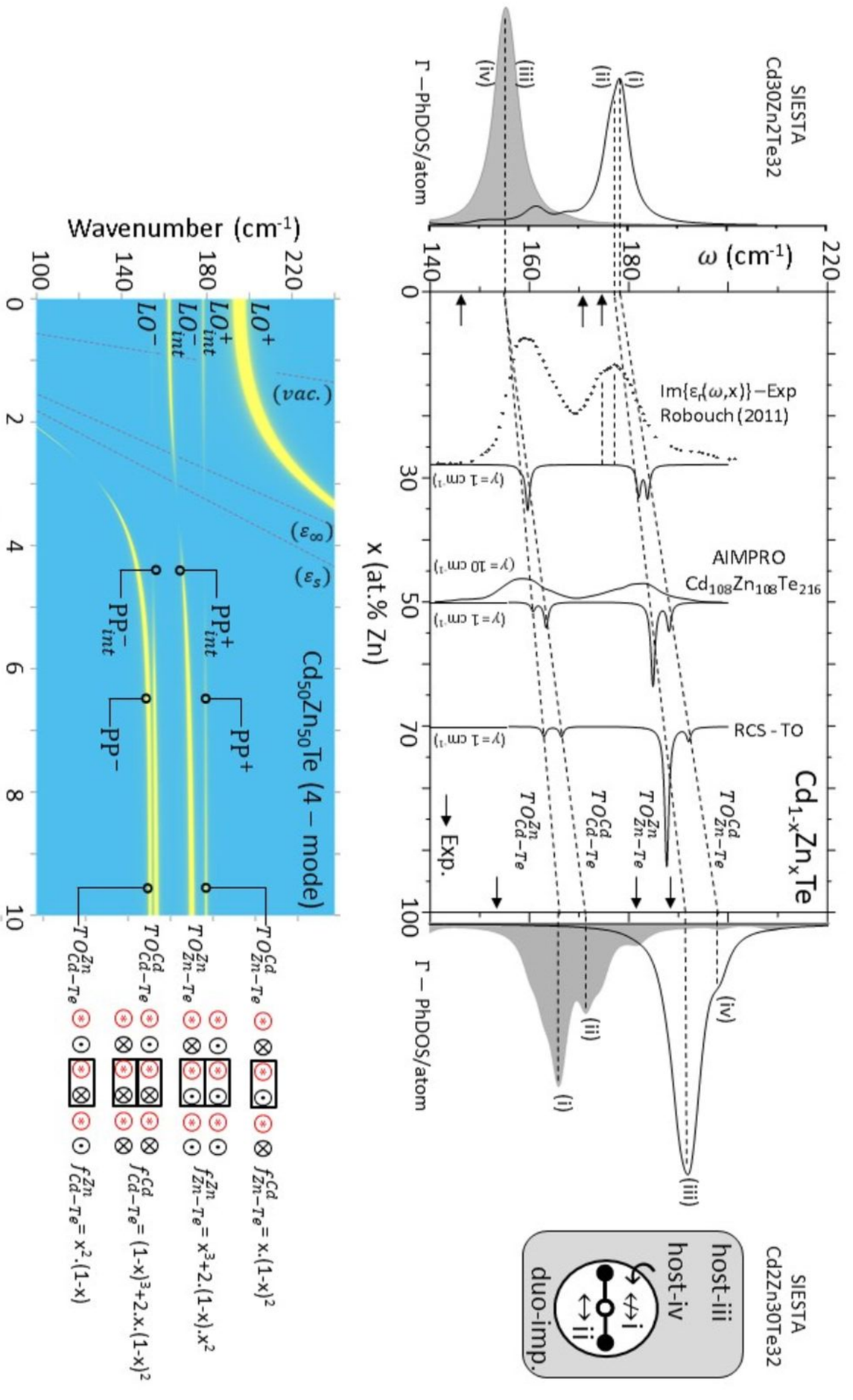

AIP Publishing

Journal of Applied Physics

ACCEPTED MANUSCRIPT

This is the author's peer reviewed, accepted manuscript. However, the online version of record will be different from this version once it has been copyedited and typeset.
PLEASE CITE THIS ARTICLE AS DOI: 10.1063/5.0134454

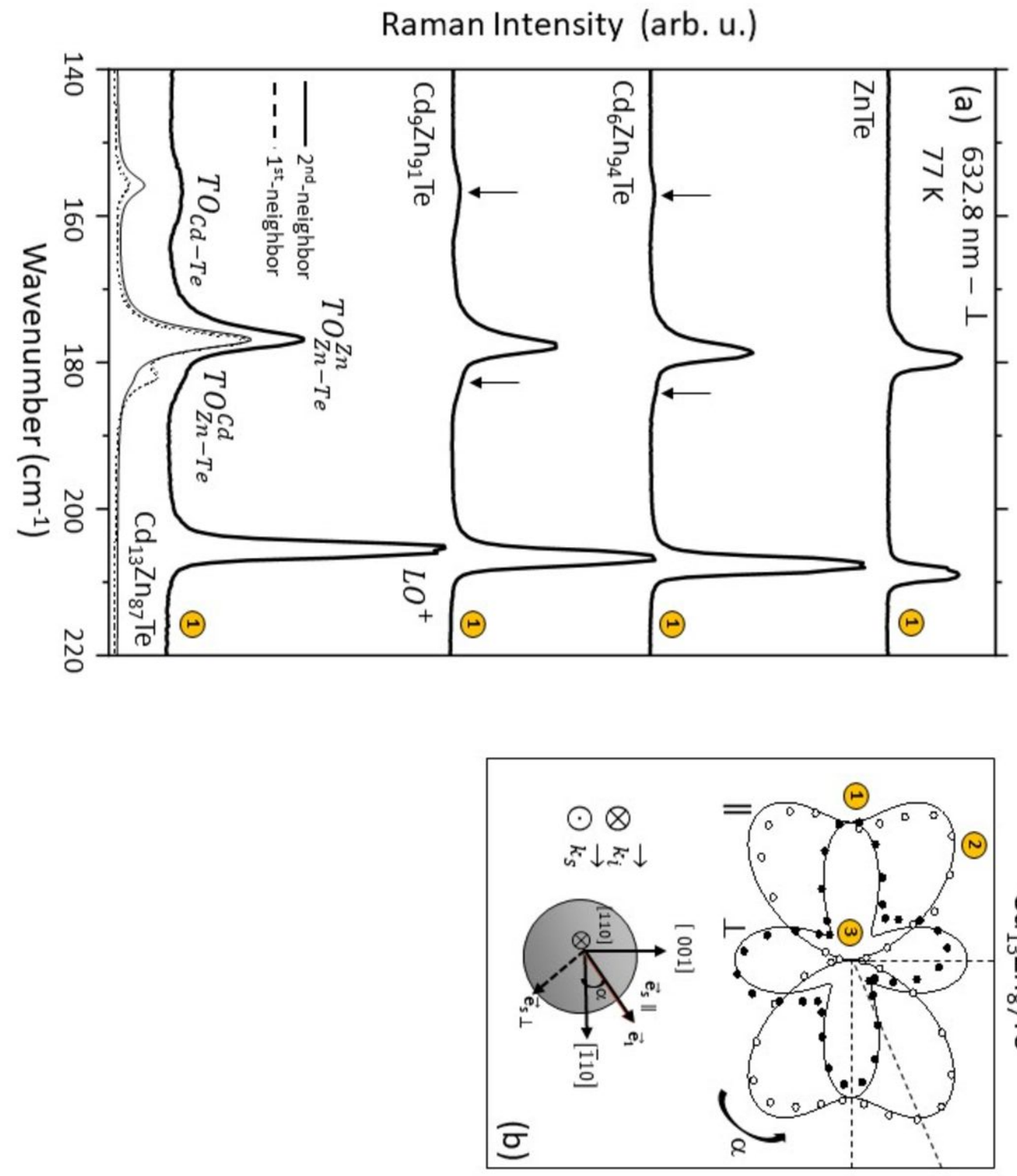

AIP Publishing

Journal of Applied Physics

ACCEPTED MANUSCRIPT

This is the author's peer reviewed, accepted manuscript. However, the online version of record will be different from this version once it has been copyedited and typeset.
PLEASE CITE THIS ARTICLE AS DOI: 10.1063/5.0134454

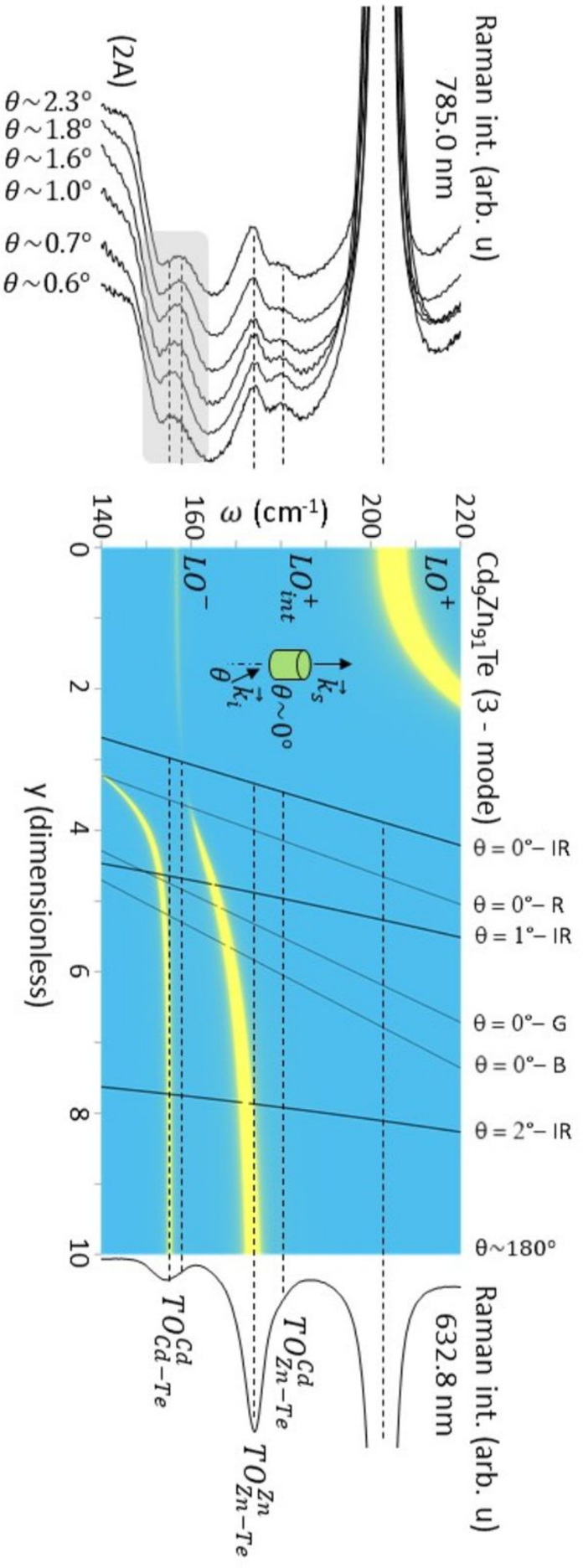

AIP Publishing

Journal of Applied Physics

PLEASE CITE THIS ARTICLE AS DOI: 10.1063/5.0134454

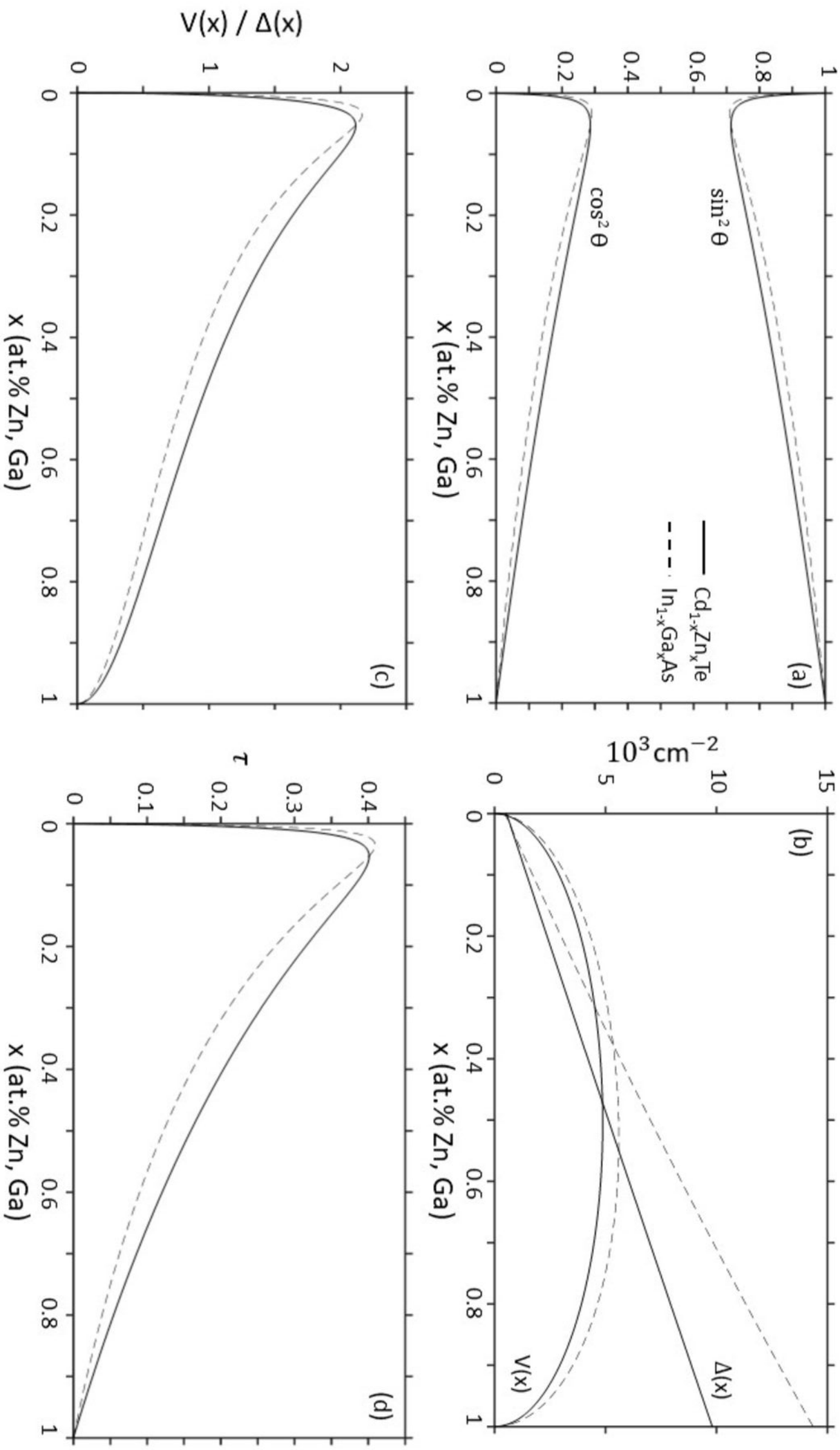

AIP Publishing
Journal of Applied Physics
ACCEPTED MANUSCRIPT

PLEASE CITE THIS ARTICLE AS DOI: 10.1063/5.0134454